



HAL
open science

Upper third molar internal structural organization and semicircular canal morphology in Plio-Pleistocene South African cercopithecoids

Amélie Beaudet, Jean Dumoncel, John Francis Thackeray, Laurent Bruxelles, Benjamin Duployer, Christophe Tenailleau, Lunga Bam, Jakobus Hoffman, Frikkie de Beer, José Braga

► To cite this version:

Amélie Beaudet, Jean Dumoncel, John Francis Thackeray, Laurent Bruxelles, Benjamin Duployer, et al.. Upper third molar internal structural organization and semicircular canal morphology in Plio-Pleistocene South African cercopithecoids. *Journal of Human Evolution*, 2016, 95, pp.104-120. 10.1016/j.jhevol.2016.04.004 . hal-01564748

HAL Id: hal-01564748

<https://hal.science/hal-01564748>

Submitted on 19 Jul 2017

HAL is a multi-disciplinary open access archive for the deposit and dissemination of scientific research documents, whether they are published or not. The documents may come from teaching and research institutions in France or abroad, or from public or private research centers.

L'archive ouverte pluridisciplinaire **HAL**, est destinée au dépôt et à la diffusion de documents scientifiques de niveau recherche, publiés ou non, émanant des établissements d'enseignement et de recherche français ou étrangers, des laboratoires publics ou privés.



Open Archive TOULOUSE Archive Ouverte (OATAO)

OATAO is an open access repository that collects the work of Toulouse researchers and makes it freely available over the web where possible.

This is an author-deposited version published in : <http://oatao.univ-toulouse.fr/>
Eprints ID : 18086

To link to this article : DOI: 10.1016/j.jhevol.2016.04.004
URL : <http://dx.doi.org/10.1016/j.jhevol.2016.04.004>

To cite this version : Beaudet, Amélie and Dumoncel, Jean and Thackeray, John Francis and Bruxelles, Laurent and Duployer, Benjamin and Tenailleau, Christophe and Bam, Lunga and Hoffman, Jakobus and de Beer, Frikkie and Braga, José *Upper third molar internal structural organization and semicircular canal morphology in Plio-Pleistocene South African cercopithecoids*. (2016) Journal of Human Evolution, vol. 95. pp. 104-120. ISSN 0047-2484

Any correspondence concerning this service should be sent to the repository administrator: staff-oatao@listes-diff.inp-toulouse.fr

Upper third molar internal structural organization and semicircular canal morphology in Plio-Pleistocene South African cercopithecoids

Amélie Beaudet^{a, b, *}, Jean Dumoncel^{b, c}, John Francis Thackeray^d, Laurent Bruxelles^{e, f, g}, Benjamin Duployer^h, Christophe Tenailleau^h, Lunga Bamⁱ, Jakobus Hoffmanⁱ, Frikkie de Beerⁱ, José Braga^{b, d}

^a Department of Anatomy, University of Pretoria, PO Box 2034, Pretoria 0001, South Africa

^b Laboratoire d'Anthropologie Moléculaire et Imagerie de Synthèse, UMR 5288 CNRS-Université de Toulouse (Paul Sabatier), 37 Allées Jules Guesde, 31 073 Toulouse Cedex 3, France

^c Institut de Recherche en Informatique de Toulouse, UMR 5505 CNRS-Université de Toulouse (Paul Sabatier), 118 Route de Narbonne, 31062 Toulouse Cedex 9, France

^d Evolutionary Studies Institute, University of the Witwatersrand, Private Bag 3, Wits 2050, Johannesburg, South Africa

^e Institut National de Recherches Archéologiques Préventives, 561 rue Etienne Lenoir, km Delta, 30900 Nîmes, France

^f Laboratoire des Travaux et Recherches Archéologiques sur les Cultures, les Espaces et les Sociétés, UMR 5608 CNRS-Université de Toulouse (Jean Jaurès), Maison de la Recherche, 5 Allées Antonio Machado, 31058 Toulouse Cedex 9, France

^g School of Geography Archaeology and Environmental Studies, University of the Witwatersrand, Private Bag 3, Wits 2050, Johannesburg, South Africa

^h Centre Inter-universitaire de Recherche et d'Ingénierie des Matériaux, UMR 5085 CNRS-Université de Toulouse (Paul Sabatier), 118 route de Narbonne, 31062 Toulouse Cedex 9, France

ⁱ South African Nuclear Energy Corporation, Pelindaba, North West Province, South Africa

A B S T R A C T

Despite the abundance of cercopithecoids in the fossil record, especially in South Africa, and the recent development of morphometric approaches, uncertainties regarding the taxonomic identification of isolated cranio-dental specimens remain. Because cercopithecoids, nearly always found in stratigraphic association with hominin remains in Plio-Pleistocene deposits, are considered as sensitive ecological and chronological biomarkers, a significant effort should be made to clarify their palaeobiodiversity by assessing additional reliable morphological diagnostic criteria. Here we test the relevance of both molar crown internal structure and bony labyrinth morphology for discrimination of fossil cercopithecoid species. We use microtomographic-based 3D virtual imaging and quantitative analyses to investigate tooth endostructural organization and inner ear shape in 29 craniodental specimens from the South African sites of Kromdraai, Makapansgat, Sterkfontein and Swartkrans and provide the first detailed description of the internal structural condition characterizing this Plio-Pleistocene primate assemblage. Our preliminary results show that enamel-dentine junction morphology could be informative for discriminating highly autapomorphic taxa such as *Theropithecus*, while semicircular canal shape is tentatively proposed as an efficient criterion for diagnosing *Dinopithecus ingens*. Further research in virtual paleoprimatology may contribute to the identification of unassigned isolated fossil remains and shed new light on the internal craniodental morphology of extinct primate taxa.

Keywords:

Old World monkeys
Primate palaeobiodiversity
Bony labyrinth
Dental internal structure
Deformation-based models
Taxonomy

1. Introduction

Old World monkeys are abundant in the Plio-Pleistocene African fossil record and are one of the best documented primate radiations (Szalay and Delson, 1979; Jablonski, 2002; Jablonski and Frost,

2010). Indeed, probably due to their adaptability, relatively fast life histories and generalized morphology, the phyletic and ecological diversification of the group significantly increased through the Plio-Pleistocene in Africa, and cercopithecoids became dominant primates during this period in Africa (Jablonski and Frost, 2010; Fleagle, 2013). More specifically, the South African karstic cave sites have yielded valuable assemblages of fossil cercopithecoids, documenting potentially seven genera and up to 12 species

* Corresponding author.

E-mail address: amelie.beaudet@univ-tlse3.fr (A. Beaudet).

(Freedman, 1957; Szalay and Delson, 1979; Delson, 1984, 1988; Jablonski, 2002; Gilbert, 2007a, 2013; McKee et al., 2011).

Because of their co-occurrence with hominins in paleontological deposits, cercopithecoids provide valuable contextual information regarding hominin paleoecology and biostratigraphic dating, as well as data for the reconstruction of pan-African dispersal patterns and palaeoenvironments (Delson, 1984, 1988; Strait and Wood, 1999; Elton, 2001; Gilbert, 2008; Bettridge and Dunbar, 2012). Also, in the absence of great apes in the Plio-Pleistocene fossil record, cercopithecoids represent the closest relatives to hominins, and they were consequently proposed as a “control-group” for the understanding of evolutionary trends and adaptations of the earliest hominins (Jolly, 1970, 2001; Elton et al., 2001; Elton, 2006). However, the use of cercopithecoids as biomarkers relies on the ability of current diagnostic criteria to taxonomically assign fossil remains and evaluate palaeobiodiversity and relative abundance.

The external craniodental morphology of extinct cercopithecoids has been widely described since the earliest discoveries in South Africa and subsequently used to define fossil cercopithecoid alpha taxonomy (e.g., Freedman, 1957; Maier, 1970; Eisenhart, 1974; Szalay and Delson, 1979; Jablonski, 2002). The most recent reviews of the material available and descriptions of new discoveries and additional specimens have used ‘traditional’ external morphological features and both clarified and expanded the currently accepted taxonomic pattern (e.g., Gilbert, 2013; Gilbert et al., 2015). However, despite the potential value of endostructural information in taxonomic studies, the internal morpho-structural condition of extinct cercopithecoid taxa is reported in only a few studies (e.g., Beaudet, 2015; Beaudet et al., 2015, 2016). If these structures prove to behave as efficient supplementary diagnostic features, their study will offer the opportunity to propose discriminators useful for the identification of isolated and fragmentary craniodental remains, which are abundant in the South African fossil record (see Brain, 1981).

1.1. Brief review of extinct South African Plio-Pleistocene cercopithecoid taxa

We follow previous published reviews of South African papionin taxa (e.g., Freedman, 1957; Szalay and Delson, 1979; Jablonski, 2002; Gilbert, 2013) recognizing four species of *Parapapio*, three species of *Papio*, one species of *Dinopithecus*, one species of *Gorgopithecus*, three subspecies of *Theropithecus oswaldi* and one species of *Cercopithecoides*. We confine our review to the taxa included and discussed in our sample.

Parapapio is currently represented in South Africa by three species (*Parapapio jonesi*, *Parapapio broomi*, and *Parapapio whitei*) initially distinguished on the basis of molar size, *Pp. whitei* having the largest and *Pp. jonesi* the smallest teeth (Broom, 1940). Morphologically, *Parapapio* differs from *Papio* by a straight profile of the muzzle dorsum rather than the steep anteorbital drop typically found in the latter (Freedman, 1957; Eisenhart, 1974). In contrast, its teeth are considered morphologically indistinguishable from those of the genus *Papio* (Freedman, 1957) or even from those of other species of Papionini (Heaton, 2006). Also, *Pp. jonesi* displays the least marked development of maxillary ridges and fossae of the *Parapapio* species (Jablonski, 2002; Heaton, 2006). The “*Parapapio*” identified at Taung, originally attributed to *Parapapio antiquus* (Freedman, 1957; Szalay and Delson, 1979), has been recently reassigned to the genus *Procercopithecus* based on shared derived features with the *Cercopithecus/Mandrillus* clade (Gilbert, 2007a, 2013). While some authors, such as Freedman (1957) and Gilbert (2013), followed the same trimodal system as Broom (1940), the validity of the species *Pp. whitei* and *Pp. jonesi* was questioned and Broom’s trichotomy challenged by others (Eisenhart, 1974; Thackeray and Myer, 2004; Heaton, 2006; Williams et al., 2007; Fourie et al., 2008).

Three extinct variants of *Papio* have been recognized in South Africa, including *Papio robinsoni*, the largest fossil species in the genus, and the two small-bodied morphs *Papio izodi* and *Papio angusticeps* (Freedman, 1957; Delson, 1984; McKee, 1993; McKee and Keyser, 1994). *Papio robinsoni* is notably characterized by a flat muzzle dorsum and the maxillary ridges raised higher than the nasal bone, whereas *P. angusticeps* has weak maxillary ridges and deep maxillary fossae and teeth shorter and broader than those of *P. robinsoni* (Freedman, 1957). The modern baboon (*Papio hamadryas sensu lato*) was suggested to have emerged from the South African fossil record (Gilbert et al., 2013).

Dinopithecus ingens is a very large and sexually dimorphic fossil baboon species found in the type locality of Schurweberg and at Swartkrans (Delson, 1984; Jablonski, 2002; Jablonski and Frost, 2010). Given numerous craniodental similarities shared with modern baboons, some authors considered *Dinopithecus* to be a subgenus of *Papio* (Freedman, 1957; Szalay and Delson, 1979; Delson and Dean, 1993; Frost, 2001; but see Gilbert, 2013). *Dinopithecus ingens* is distinguished from other papionins by a robust and rugged skull with strong masticatory apparatus, long muzzle and broad interorbital region (Freedman, 1957).

Gorgopithecus major is a large form of baboon characterized by a relatively short, high and narrow muzzle with deep maxillary and mandibular fossae, nearly vertical zygoma and slight sexual dimorphism in the skull (Freedman, 1957; Jablonski and Frost, 2010). This baboon taxon, identified at Kromdraai and Swartkrans (Delson, 1984, 1988), but also in eastern Africa (Gilbert et al., 2016), has been suggested to be phylogenetically related to extant *Lophocebus* (Gilbert, 2013).

The genus *Theropithecus* is distinguished from other papionins especially through its high crowned and columnar-cusped cheek teeth with infoldings of thick enamel and several postcranial features that are related to its terrestrial life (Jolly, 1972; Jablonski, 1993). The species *T. oswaldi* forms a chronolineage divided into three chronosubspecies: from oldest to youngest *Theropithecus oswaldi darti*, *Theropithecus oswaldi oswaldi* and *Theropithecus oswaldi leakeyi* (Leakey, 1993; Frost and Delson, 2002; Frost, 2007). *Theropithecus oswaldi darti* is found at Makapansgat, while *T. o. oswaldi* is known at Swartkrans and Sterkfontein (Jablonski, 1993). *Theropithecus oswaldi leakeyi* was identified at Hopefield (Dechow and Singer, 1984) and Bolt’s Farm Pit 10 (Gilbert, 2007b).

The extinct colobine species *Cercopithecoides williamsi* is spatially and temporally largely distributed in South African Plio-Pleistocene sites (e.g., Kromdraai, Makapansgat, Sterkfontein, Swartkrans, Taung) (Delson, 1984, 1988; Jablonski, 2002). The cranium displays diagnostic traits such as a rounded calvarium, short and relatively narrow muzzle, and a wide face with large interorbital distance (Freedman, 1957; Jablonski, 2002; key features reviewed in McKee et al. 2011). Teeth are small and exhibit typical colobine features (Szalay and Delson, 1979).

1.2. Internal craniodental structures as potential diagnostic criteria

Dental remains are usually the most common material in the primate fossil record (Hartwig, 2002). The identification of isolated teeth or dentognathic fragments is difficult because there are often no distinctive morphological features that can be used to accurately distinguish between closely related taxa. In association with significant improvements in analytical tools, the development of advanced imaging techniques (such as micro-focus X-ray tomography) permits the noninvasive extraction of a wide range of morphostructural information (reviewed in Macchiarelli et al., 2013).

Primate enamel thickness variations were previously suggested to be explained by advantages for resisting fracture and abrasion or for shearing (e.g., Gantt, 1977; Kay, 1981; Dumont, 1995). More

recently, the possibility that thick enamel might be adaptive in seasonal environments was suggested, based on the assessment of enamel thickness variations in macaques (Kato et al., 2014). In addition to functional hypotheses, enamel thickness variations recorded in fossil hominins have also been reported to provide potential phylogenetic and taxonomic information (e.g., Olejniczak et al., 2008a,b). While data on dental tissue volumes and proportions have been documented for extant cercopithecoid taxa, they have mainly been used as part of a comparative sample (e.g., Gantt, 1977; Kay, 1981; Dumont, 1995; Shellis et al., 1998; Hlusko et al., 2004; Grine et al., 2005; Olejniczak et al., 2008c; McGraw et al., 2012; Kato et al., 2014), and little is known about fossil specimens (Beaudet, 2015; Beaudet et al., 2015, 2016). This consequently limits the potential taxonomic inferences that can be made from dental tissue proportions for cercopithecoids. In addition to the tissue proportions, enamel-dentine junction (EDJ) morphology is another aspect of internal dental structure that is thought to include a phylogenetic signal and has proved to be useful in the diagnosis of fossil hominoid species (e.g., Skinner et al., 2008; Zanolli et al., 2012, 2014). Previous 2D investigations of cercopithecoid EDJ shape described a specific pattern in comparison with other anthropoids but did not explore discrimination beyond the superfamily level (Olejniczak et al., 2004, 2007).

The extraction and characterization of the bony labyrinth has also provided significant taxonomic and phylogenetic information in primates (e.g., Spoor, 1993; Spoor et al., 2003; Rook et al., 2004; Lebrun et al., 2010; Gunz et al., 2012; Braga et al., 2013, 2015). As the inner ear is part of the hearing and balance systems, subtle morphological variations and allometric deviations reported may be correlated with hearing capacities (e.g., Manoussaki et al., 2008; Kirk and Gosselin-Ildari, 2009; Braga et al., 2015) or locomotor behaviours (e.g., Spoor et al., 2007; Silcox et al., 2009; Malinzak et al., 2012). More specifically, dimensions and angular measurements assessed for the semicircular canals were proposed as proxies for the reconstruction of agility (Spoor et al., 2002; Malinzak et al., 2012), but inner ear shape characterized by geometric morphometric analyses was nonetheless revealed to be relevant for detecting phylogenetic signal in strepsirrhines (Lebrun et al., 2010).

By using techniques of three-dimensional virtual imaging and high resolution quantitative characterization, coupled with morphometric analyses, we investigated internal morphological features in Plio-Pleistocene South African cercopithecoid samples and living relatives. We compared our 3D-based results to the current taxonomy and evaluated the potential of dental and semicircular canal (SCC) features as diagnostic criteria for discriminating extinct taxa. Accordingly, here we consider the hypothesis that dental endostructures and inner ear features provide taxonomically diagnostic information for the identification of fossil cercopithecoid remains. Specifically, we apply this to the well-studied *Parapapio* and *Papio* taxa, and we consequently include additional tests for exploring the morphological variability of these two groups and evaluate the sensitivity of our criteria. Finally, the combination of dental endostructural properties and inner ear morphology offers the unique opportunity to compare the potential of these structures for species diagnosis.

2. Material and methods

2.1. Sample and data collection

Our fossil sample includes 29 cercopithecoid specimens from four South African Plio-Pleistocene sites (Kromdraai, Makapansgat, Sterkfontein, Swartkrans) representing *Pp. jonesi*, *Pp. broomi*, *Pp. whitei*, *Parapapio* sp., *Papio angusticeps*, *P. robinsoni*, *Papio* sp.,

D. ingens, *G. major*, *T. o. oswaldi*, *T. o. darti* and *C. williamsi* (Table 1). Our comparative sample of extant specimens is detailed in Table 1. All the specimens investigated in this study have been imaged by micro-focus X-ray tomography (μ CT) using various systems detailed in Table 1. The isometric voxel size of the reconstructed volumes ranges from 18.7 to 122.9 μ m (Table 1).

We obtained dental tissue proportions and SCC surfaces through semi-automatic threshold-based segmentations and 3D mesh reconstructions via the software Avizo v8.0 (Visualization Sciences Group Inc.). The sample sizes of the dental tissue proportions and EDJs investigated, plus SCCs extracted, are listed in Table 1. For internal dental structure, teeth with dentine horns affected by wear were excluded from the overall tissue proportion analyses. The enamel topographic distribution documented in each taxon was imaged by colour maps from dark blue (thin) to red (thick) in the best-preserved specimens. Conversely, the overall available dental sample was used to assess the lateral enamel thickness and distribution. Finally, teeth displaying a degree of wear exceeding stage 9C in the score system developed by Delson (1973) were excluded from the analysis of the EDJ shape. This stage of wear corresponds to a maximum loss of around 5% of the total enamel-dentine junction surface (estimation based on the specimen KA 194 which presents the highest degree of wear).

2.2. 3D dental tissue proportions and enamel distribution

We measured our dental parameters on the upper third molars (UM3) due to their lesser degree of wear compared to the other elements of the postcanine dentition. The dental crown was separated from the roots by virtually closing the enamel cap, following the curved cervical boundary (“Fill hole” module available on Avizo v8.0). This coronal volume embeds both the dentine material and pulp cavity. In addition to the overall crown, we evaluated the lateral aspect of the enamel thickness by virtually removing all the tooth occlusal to the deepest point of the enamel-dentine junction through a plane parallel to the cervix line (Toussaint et al., 2010; Benazzi et al., 2011; Macchiarelli et al., 2013). Three variables were measured in each specimen and for both the overall crown and the lateral portion: volume of the enamel cap (V_e , mm^3), volume of the coronal dentine that includes the coronal aspect of the pulp chamber (V_{cdp} , mm^3), and surface of the enamel-dentine junction ($SEDJ$, mm^2). We then calculated two indices of enamel thickness: 3D average enamel thickness (3D AET, mm) calculated as the ratio between V_e and $SEDJ$, and 3D relative enamel thickness (3D RET) obtained through the ratio $AET/(V_{cdp})^{1/3} \cdot 100$ and allowing direct, scale-free comparisons (Kono, 2004; Olejniczak et al., 2008a). Intra- and inter-observer tests for measurement accuracy run by two observers in previous published studies using a similar analytical protocol revealed differences less than 5% (cf. Bondioli et al., 2010; Zanolli et al., 2014).

We detailed the 3D distribution of enamel across the UM3s by computing the distances between the occlusal and the enamel-dentine junction surfaces through the “Surface Distance” module on Avizo v8.0. The distances recorded were visualized at the outer enamel surface using a colour scale ranging from dark blue (“thinner”) to red (“thicker”) (Macchiarelli et al., 2008, 2013; Bayle et al., 2011).

2.3. Enamel-dentine junction morphology

To compare the EDJs among species, we used a landmark-free method that relies on the construction of group-average surface models and their deformation to the investigated surfaces (Durrleman et al., 2012a,b; Dumoncel et al., 2014). Surfaces are represented by a set of oriented faces and the comparison does not assume a point-to-point correspondence between samples as in

Table 1List of the Plio-Pleistocene and extant cercopithecoid specimens/samples detailed by micro-focus X-ray tomography (μ CT) and used for assessing tooth structural variation, tissue proportions and inner ear morphology.^a

| | Specimen/sample | Site/provenance* | Source | Stored at | μ CT equipment | μ CT acquisition voxel size (μ m) | Elements | | | |
|--|-----------------|---|---|---|--|--|------------|---------|-----|----|
| | | | | | | | UM3 crown | UM3 EDJ | SCC | |
| Fossil taxa | | | | | | | | | | |
| <i>Parapapio jonesi</i> | n = 1 | STS 565 | Sterkfontein (Member 4) | Freedman (1957), Eisenhart (1974), Brain (1981), Jablonski (2002) | Ditsong ^b | Necsa ¹ | 71.9 | 1 | – | 1 |
| <i>Parapapio broomi</i> | n = 5 | MP 224**, STS 251, STS 354, STS 544, STS 564 | Makapansgat (Member 4) Sterkfontein (Member 4) | Freedman (1957, 1976), Eisenhart (1974), Brain (1981), Jablonski (2002), Heaton (2006), Williams et al. (2007), Gilbert (2013) | Ditsong ^b Wits ^c | Necsa ¹ Pal. Centre ² | 30.5–81.6 | 2 | 4 | 2 |
| <i>Parapapio whitei</i> | n = 3 | MP 221**, STS 370B, STS 370C | Makapansgat (Member 4) Sterkfontein (Member 4) | Freedman (1957, 1976), Brain (1981), Jablonski (2002), Gilbert (2013) | Ditsong ^b Wits ^c | Necsa ¹ Pal. Centre ² | 37.7–71.2 | 1 | 2 | 2 |
| <i>Parapapio</i> sp. | n = 2 | M 3133**, MP 208 | Makapansgat (Member 4) | Williams et al. (2007), Fourie et al. (2008) | Wits ^c | Pal. Centre ² | 78.7 | – | – | 2 |
| <i>Papio angusticeps</i> | n = 1 | KA 194 | Kromdraai A | Freedman (1957), Brain (1981), Gilbert (2013) | Ditsong ^b | Necsa ¹ | 74.0 | 1 | 1 | – |
| <i>Papio robinsoni</i> | n = 4 | SK 536, SK 555, SK 562, SK 602 | Swartkrans (Member 1) | Freedman (1957), Freedman and Brain (1977), Brain (1981), Jablonski (2002) | Ditsong ^b | Necsa ¹ | 44.9–86.6 | 4 | 4 | – |
| <i>Papio</i> sp. | n = 1 | Swartkrans 3*** | Swartkrans | Ditsong catalogue; this study | Ditsong ^b | Necsa ¹ | 39.4 | 1 | 1 | – |
| <i>Dinopithecus ingens</i> | n = 2 | SK 554, SK 599 | Swartkrans (Member 1) | Freedman (1957), Brain (1981) | Ditsong ^b | Necsa ¹ | 88.3–95.7 | – | – | 2 |
| <i>Gorgopithecus major</i> | n = 2 | KA 192, KA 193 | Kromdraai A | Freedman (1957), Brain (1981), Jablonski (2002) | Ditsong ^b | Necsa ¹ | 18.7–63.6 | 2 | 1 | – |
| <i>Theropithecus oswaldi oswaldi</i> | n = 1 | SK 561 | Swartkrans (Member 1) | Freedman (1957), Freedman and Brain (1977), Brain (1981), Jablonski (2002) | Ditsong ^b | Necsa ¹ | 99.9 | 1 | 1 | 1 |
| <i>Theropithecus oswaldi darti</i> | n = 2 | M 3073, MP 222 | Makapansgat (Member 4) | Maier (1972), Freedman (1976), Jablonski (2002), Jablonski and Frost (2010) | Wits ^c | Pal. Centre ² | 71.2 | 1 | 2 | 2 |
| <i>Cercopithecoides williamsi</i> | n = 5 | M 3055, MP 3/ M 203/AD 1326-3, MP 36/M 236/AD 1326-6, STS 252, STS 559A | Makapansgat (Member 4) Sterkfontein (Member 4) | Mollett (1947), Freedman (1957), Maier (1970), Eisenhart (1974), Brain (1981), Jablonski (2002), Heaton (2006), Fourie et al. (2008), McKee et al. (2011) | Ditsong ^b Wits ^c | Necsa ¹ Pal. Centre ² | 51.4–78.7 | 1 | 1 | 5 |
| Extant taxa | | | | | | | | | | |
| <i>Papio</i> (<i>anubis</i> n = 8, <i>cynocephalus</i> n = 2, <i>cynocephalus kindae</i> n = 5, <i>hamadryas</i> n = 3, <i>ursinus</i> n = 3) | n = 21 | | Central Africa, Congo, Ethiopia, Mozambique, Zambia, unknown provenance | | MNHN ^d MRAC ^e AMNH ^f MHNT ^g UT-PS ^h | AST-RX ³ FERMaT ⁴ MIF ⁵ MEDES ⁶ SEMATEC ⁷ | 33.0–122.9 | 7 | 7 | 21 |
| <i>Theropithecus gelada</i> | n = 3 | | Ethiopia | | MNHN ^d AMNH ^f | AST-RX ³ MIF ⁵ | 35.0–95.7 | 2 | 2 | 3 |
| <i>Lophocebus albigena</i> | n = 4 | | Cameroon, Congo, Gabon | | MNHN ^d MRAC ^e | AST-RX ³ FERMaT ⁴ | 33.0–66.2 | 4 | 4 | 4 |
| <i>Mandrillus</i> (<i>leucophaeus</i> n = 3, <i>sphinx</i> n = 3) | n = 6 | | Cameroon, Guinea | | MRAC ^e MHNT ^g | FERMaT ⁴ MEDES ⁶ | 33.0–41.0 | 2 | 2 | 6 |
| <i>Cercocebus</i> (<i>atys</i> n = 2, <i>torquatus</i> n = 2) | n = 4 | | Cameroon, Liberia | | MRAC ^e | FERMaT ⁴ MEDES ⁶ | 33.0–41.0 | 3 | 2 | 4 |
| <i>Macaca</i> (<i>mulatta</i> n = 1, <i>nigra</i> n = 1, <i>radiata</i> n = 1, <i>sylvanus</i> n = 4, sp. n = 1) | n = 8 | | India, Senegal, unknown provenance | | AMNH ^f MHNT ^g | FERMaT ⁴ MIF ⁵ MEDES ⁶ SEMATEC ⁷ | 33.0–41.0 | 3 | 3 | 8 |
| <i>Cercopithecus</i> (<i>cephus</i> n = 2, <i>halmyni</i> n = 1, <i>mona</i> n = 1) | n = 4 | | Congo, Guinea | | MHNT ^g | FERMaT ⁴ MEDES ⁶ | 33.0–41.0 | 1 | 1 | 4 |

(continued on next page)

Table 1 (continued)

| Specimen/sample | Site/provenance* | Source | Stored at | µCT equipment | µCT acquisition voxel size (µm) | Elements | | |
|---|--|--------|--|---|---------------------------------|-----------|---------|-----|
| | | | | | | UM3 crown | UM3 EDJ | SCC |
| <i>Erythrocebus patas</i> n = 2 | Congo, Senegal | | MRAC ^c MHNT ^g | FERMat ^d | 33.0 | 1 | 2 | 1 |
| <i>Chlorocebus (aethiops)</i> n = 3, <i>pygerythrus</i> n = 2 | Congo, Republic of Cabo Verde, Senegal, South Africa | | MRAC ^c MHNT ^g | FERMat ^d | 33.0 | 4 | 4 | 5 |
| <i>Colobus (angolensis)</i> n = 15 | Congo, Ethiopia, unknown provenance (n = 4) | | MNHN ^d MRAC ^c AMNH ^f MHNT ^g | AST-RX ³ FERMat ^d MIF ⁵ MEDES ⁶ SEMATEC ⁷ | 33.0–66.2 | 5 | 7 | 15 |
| <i>Pliocolobus (baduus)</i> n = 7 | Congo, unknown provenance (n = 2) | | MRAC ^c AMNH ^f | FERMat ^d MIF ⁵ MEDES ⁶ | 33.0–41.0 | 1 | 1 | 7 |

^aUM3: third upper molar; EDJ: enamel dentine-junction; SCC: semicircular canal. ^bDitsong National Museum of Natural History, Pretoria; ^cUniversity of the Witwatersrand, Johannesburg; ^dMuséum national d'Histoire naturelle, Paris; ^eMusée royal de l'Afrique centrale, Tervuren (some specimens are published in [Braga et al., 2015](#)); ^fAmerican Museum of Natural History, New York; ^gMuseum d'Histoire naturelle de Toulouse (some specimens are published in [Braga et al., 2015](#)); ^hUniversité de Toulouse, Paul Sabatier ([Braga et al., 2015](#)).

ⁱSouth African Nuclear Energy Corporation, Pretoria ([Hoffman and de Beer, 2012](#)); ²Palaeosciences Centre, University of the Witwatersrand, Johannesburg; ³Accès Scientifique à la Tomographie à Rayons-X, MNHN, Paris; ⁴Fluides Energie Réacteurs Matériaux et Transferts, Toulouse; ⁵Microscopy and Imaging Facility, AMNH, New York (data provided by Pr Eric Delson and the AMNH Department of Mammalogy, some specimens were downloaded from [www.morphosource.org](#), Duke University); ⁶Institut de Médecine et de Physiologie Spatiales, Toulouse ([Braga et al., 2015](#)); ⁷Sematec Metrology, Oyonnax ([Braga et al., 2015](#)).

⁸Unless mentioned, the specimens from Sterkfontein and Swartkrans derive from Member 4 and Member 1 respectively and those from Makapansgat are from Member 4 ([Brain, 1981](#); [Heaton, 2006](#)). ⁹Uncertain stratigraphic localization but an attribution to Member 4 is proposed by the catalogue of the University of the Witwatersrand for M 3133, and the descriptions of MP 221 and MP 224 by [Freedman \(1976\)](#) suggest an origin in Member 4.

¹⁰No previous publications are known for the specimen Swartkrans 3 labelled as *Papio* sp. in the catalogue.

classical landmark-based geometric morphometric analyses. The deformations between surfaces are mathematically modelled as a “diffeomorphism”, i.e., a one-to-one deformation of the 3D space that is smooth, invertible and with a smooth inverse, which is particularly appropriate for comparing overall shapes and local orientation in the field of computational anatomy ([Glaunès and Joshi, 2006](#); [Durrleman et al., 2014](#)). From a set of surfaces, a mean shape, together with a set of initial control points located near its most variable parts, and a set of momenta parameterizing the deformations of the mean shape to each individual, are estimated.

As a pre-processing step, unscaled EDJs were aligned, using the “Align Surface” module available on the software Avizo v8.0. Based on the deformation framework, we generated (i) a global mean shape (GMS) associated with a set of deformations from the GMS to each EDJ (hereinafter called “GMS-to-individuals”), computed from our complete sample, and (ii) a taxon mean shape (TMS) for each genus investigated in our study (except for the groups represented by one isolated individual, e.g., *G. major* and *C. williamsi*) representing the deformation from the TMS and using the sample mean of the momenta recorded within the group ([Fig. 1](#)). Because it has been argued that teeth of *Parapapio* can be not be distinguished from those of *Papio* ([Freedman, 1957](#); [Heaton, 2006](#)), we tentatively grouped the individuals together and performed analyses to explore the morphological variability of the two combined groups. In addition to GMS-to-individuals deformations, the GMS was also deformed to the TMS (hereinafter called “GMS-to-TMS”). [Figure 1](#) illustrates how the GMS was deformed through the GMS-to-TMS process with a scale of displacements ranging from 0 to 1.5 mm.

Intraspecific and intrageneric variations were explored by performing a principal component analysis using the deformation momenta from TMS to individuals (hereinafter called “TMS-to-individuals”) ([Durrleman, 2010](#)). Deformations along the two first axes illustrate how the TMS varies within the population from the mean to one time the standard deviation (σ) (i.e., the square root of the corresponding eigenvalue). We particularly explored the variability of the *Parapapio* and *Papio* groups ([Fig. 2](#)).

The magnitude of displacements recorded during the deformation process (i.e., GMS-to-individuals, GMS-to-TMS and TMS-to-individuals) were rendered by colour maps from dark blue (lowest values) to red (highest values) onto the EDJ surfaces (i.e., individual EDJ, TMS or $\pm\sigma$) ([Figs. 1–2](#)).

2.4. Semicircular canal morphology

We investigated the morphology of the SCCs by using a semilandmark-based three-dimensional geometric morphometric approach ([Gunz et al., 2012](#)). Four curves placed along the outer inner ear surface were defined by semilandmark sets as follow: one along the common crus (formed by four equally spaced semilandmarks) and one for each SCC (20 equally spaced semilandmarks per canal). These four curves were delimited by landmarks located at the entrance of the common crus into the vestibule, the junction between the anterior and the posterior SCCs, the entrance of the three ampullae into the vestibule, and the entrance of the lateral semicircular canal into the vestibule. The conformations of the SCCs were comparatively assessed through a generalized Procrustes analysis (GPA; [Bookstein, 1991](#)).

2.5. Exploratory multivariate analysis

To test the contribution of internal craniodental structures for the diagnosis of cercopithecoid taxa, morphological variations recorded for each structure were statistically explored and their potential in discriminating groups evaluated. As a preliminary approach, we focused our study at the genus level. Accordingly, we

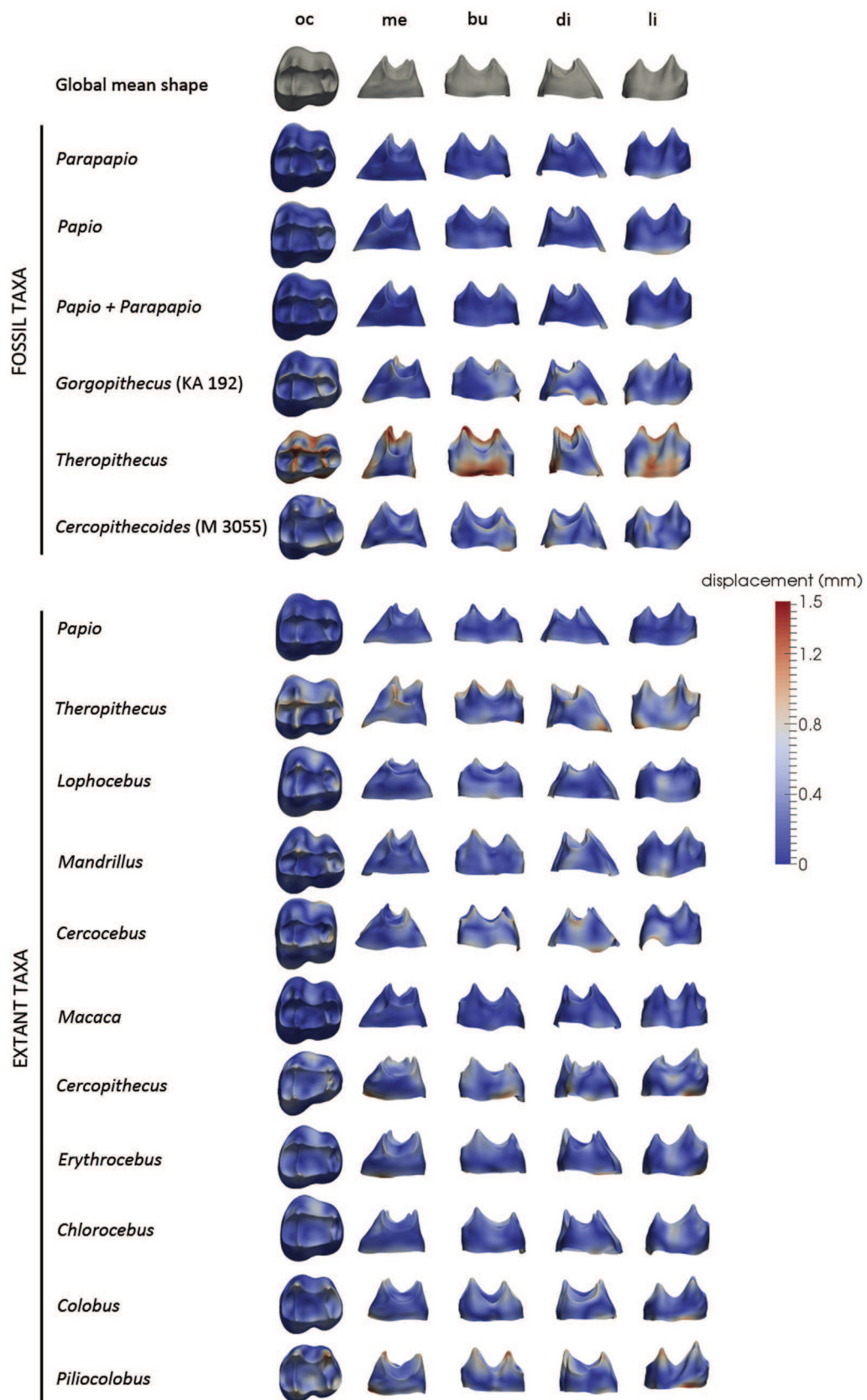


Figure 1. Comparative maps of morphological deformations from the mean template (GMS; top row) of the upper third molar enamel-dentine junctions (EDJs) computed for the overall cercopithecoid sample to the taxon mean shape (TMS) of Plio-Pleistocene and extant investigated taxa/groups. Regardless of their original side, all EDJs are shown as right and are imaged in occlusal (oc), mesial (me) buccal (bu), distal (di), and lingual (li) views. Cumulative displacement variations are rendered by a pseudo-colour scale ranging from dark blue (lowest values) to red (highest values).

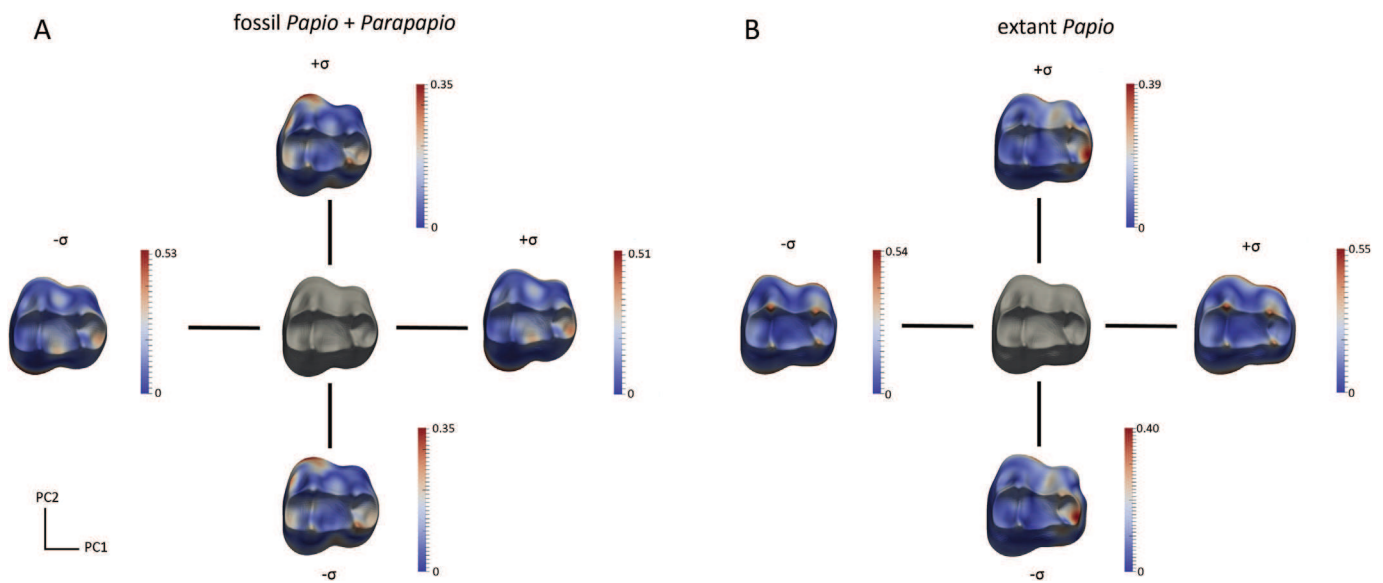


Figure 2. Morphological standard deviation of the taxon mean shape (TMS; in grey) of the upper third molar enamel-dentine junctions along the two axes computed for the Plio-Pleistocene group including both *Papio* and *Parapapio* (A) and for the extant *Papio* sample (B). Cumulative displacement variations (in mm) are rendered by a pseudo-colour scale ranging from dark blue (lowest values) to red (highest values).

performed a between-group principal component analysis (bgPCA) on both the GMS-to-individuals EDJ deformations and the Procrustes analysis of the SCCs. By projecting the data onto the principal components of the group means, the bgPCA is considered more efficient in assessing group separation in biology than the ordinary principal component analyses (Mitteroecker and Bookstein, 2011).

Results of the GPA computed for the semilandmarks placed along the SCCs and distances computed between EDJ surfaces were also described by a canonical variate analysis (CVA). The CVA is a multivariate classification technique that maximizes the ratio of the between-group sum of squares to the within-group sum of squares through a discriminant function (Gittins, 1985). Given the comparative value of such analysis for statistical populations, we

described the major trends in the distribution of groups in the shape space. Instead of being considered as a tool for discrimination, CVA is informative for interpreting the similarities shared by the groups constituted a priori.

A hierarchical clustering on principal components (HCPC) was performed using the GMS-to-individuals deformations with the package FactoMineR (Lê et al., 2008) for R v.3.2.1 (R Development Core Team, 2015). A hierarchical tree (or dendrogram) was obtained from the decomposition of the total variance (inertia) in between- and within-group variance. Contrary to the bgPCA or the CVA, the HCPC does not require any a priori classification and specimens are aggregated into clusters according to the distances (similarities) recorded between them.

Table 2
3D crown tissue proportions (including average and relative enamel thickness) of the third upper molar in some Plio-Pleistocene and extant cercopithecoid specimens/samples.^a

| Specimen/sample | | Ve (mm ³) | Vcdp (mm ³) | SEDJ (mm ²) | 3D AET (mm) | 3D RET |
|----------------------------|--------------|-----------------------|-------------------------|-------------------------|-------------|-----------|
| Fossil taxa | | | | | | |
| <i>Pp. broomi</i> | STS 544 | 191.8 | 238.0 | 215.0 | 0.9 | 14.4 |
| | MP 224 | 248.2 | 254.7 | 218.1 | 1.1 | 18.0 |
| | mean | 220.0 | 246.4 | 216.5 | 1.0 | 16.2 |
| | | | | | | |
| <i>P. robinsoni</i> | SK 536 | 427.7 | 541.5 | 374.0 | 1.1 | 14.0 |
| | SK 602 | 343.2 | 447.0 | 321.2 | 1.1 | 14.0 |
| | mean | 385.4 | 494.3 | 347.6 | 1.1 | 14.0 |
| <i>Papio</i> sp. | Swartkrans 3 | 282.1 | 372.7 | 286.5 | 1.0 | 13.7 |
| <i>C. williamsi</i> | M 3055 | 129.9 | 196.3 | 177.6 | 0.7 | 12.6 |
| Extant taxa | | | | | | |
| <i>Papio</i> (n = 4) | mean | 232.4 | 237.2 | 205.9 | 1.1 | 18.2 |
| | range | 163.6–285.4 | 159.0–281.0 | 167.4–231.5 | 1.0–1.2 | 17.3–18.8 |
| <i>Lophocebus</i> (n = 3) | mean | 44.3 | 48.8 | 64.6 | 0.7 | 18.7 |
| | range | 37.6–50.5 | 42.3–54.2 | 58.7–69.1 | 0.6–0.7 | 18.3–19.3 |
| <i>Mandrillus</i> (n = 1) | | 159.5 | 198.7 | 204.1 | 0.8 | 13.4 |
| <i>Cercocebus</i> (n = 3) | mean | 98.6 | 107.1 | 119.0 | 0.8 | 17.4 |
| | | 80.3–118.7 | 90.1–132.2 | 110.0–134.3 | 0.7–0.9 | 15.9–19.1 |
| <i>Macaca</i> (n = 2) | mean | 90.4 | 100.5 | 123.8 | 0.7 | 15.8 |
| | range | 75.0–105.8 | 74.7–126.3 | 106.8–140.7 | 0.7–0.8 | 15.0–16.7 |
| <i>Chlorocebus</i> (n = 4) | mean | 33.6 | 45.1 | 66.3 | 0.5 | 14.3 |
| | range | 27.3–40.4 | 32.6–50.4 | 53.5–72.6 | 0.4–0.6 | 11.5–16.0 |
| <i>Colobus</i> (n = 2) | mean | 49.8 | 58.0 | 81.1 | 0.6 | 16.0 |
| | range | 49.5–50.1 | 52.5–63.5 | 74.7–87.6 | 0.6–0.7 | 14.3–17.7 |

^a See text (Material and methods) for variable abbreviations. Data for the specimens STS 544, MP 224, SK 602, M 3055 are from Beaudet et al. (2016).

3. Results

3.1. 3D dental tissue proportions and enamel distribution

Estimates of whole crown tissue proportions for the UM3 in Plio-Pleistocene and extant cercopithecoïd specimens/samples are shown in Table 2 and Figure 3A. The 3D AET separates fossil *Papio*, extant *Papio* and *Parapapio* (with their higher average values) from *Mandrillus* and the small-bodied extant *Lophocebus*, *Cercocebus*, *Macaca*, *Erythrocebus*, *Ptilocolobus* and *Colobus*. The

C. williamsi values fall within extant variation of *Macaca* and both *Cercocebus* and *Lophocebus*. The scale-free 3D RET is globally higher for extant *Papio*, *Lophocebus* and *Cercocebus* when compared to other living and fossil taxa (Fig. 3A). Because Swartkrans 3 was attributed at the genus level only, we did not include it in the comparative plots but its values, similar to those of *P. robinsoni*, are shown in Table 2.

Estimates of tissue proportions recorded in the lateral tooth portion are given in Table 3 and Figure 3B. As for the whole crown proportions, the fossil taxa (including *Theropithecus*, *Papio*,

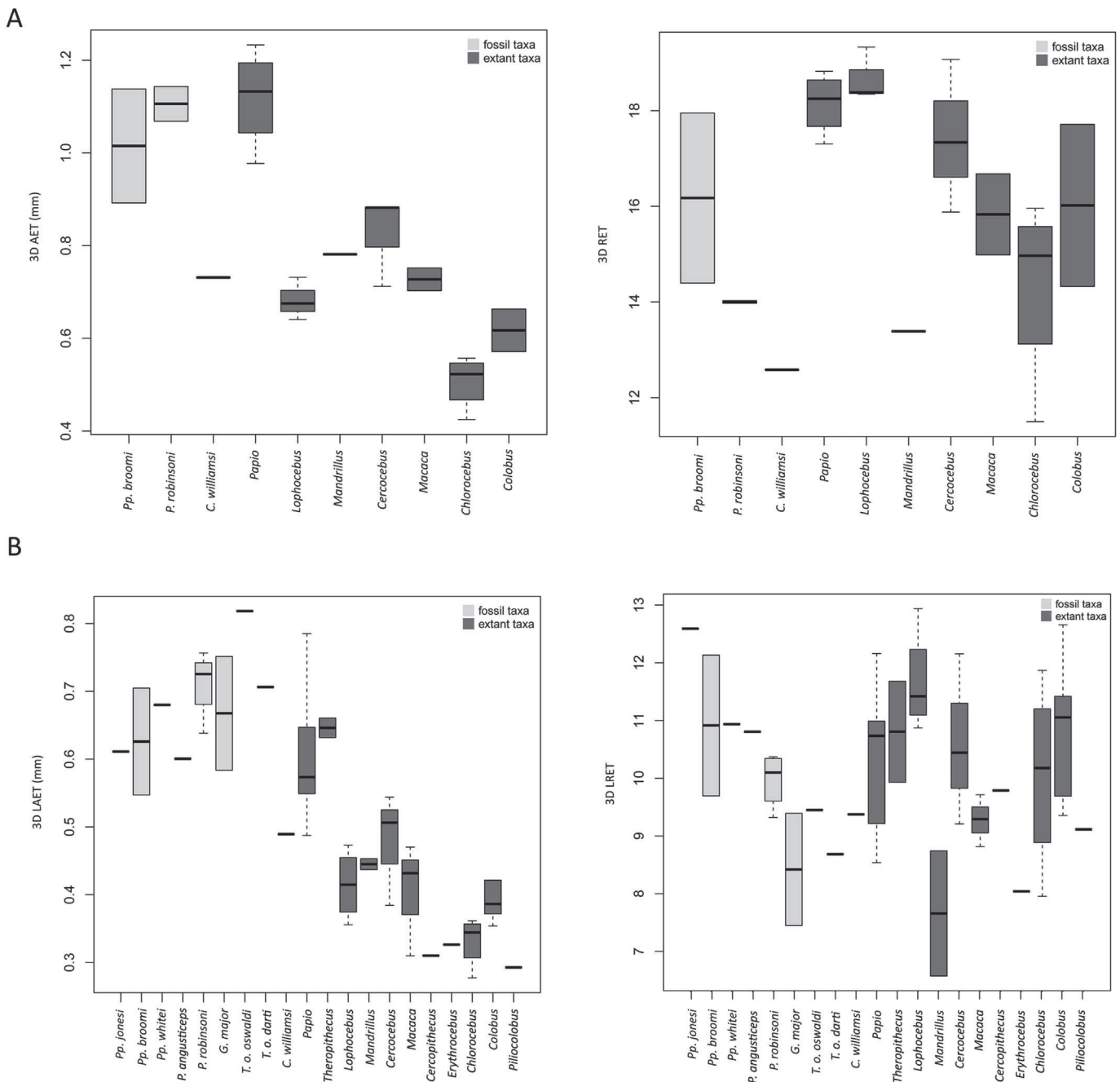


Figure 3. Boxplot of 3D tooth tissue proportions in the overall (A) and lateral aspect (B) of the upper third molar crown in some Plio-Pleistocene and extant cercopithecoïd specimens/samples. 3D AET: 3D average enamel thickness; 3D RET: 3D relative enamel thickness; 3D LAET: 3D lateral average enamel thickness; 3D LRET: 3D lateral relative enamel thickness. Each boxplot presents the data minimum (i.e., lowest horizontal bar), the first quartile (i.e., lower edge of the box), median (i.e., bar inside the box), third quartile (i.e., upper edge of the box), and data maximum (i.e., highest bar).

Table 3
3D crown tissue proportions (including average and relative enamel thickness) of the lateral aspect of the upper third molar in some Plio-Pleistocene and extant cercopithecoïd specimens/samples.^a

| Specimen/sample | | Vle (mm ³) | Vlcp (mm ³) | SEDJL (mm ²) | 3D LAET (mm) | 3D LRET |
|------------------------------|--------------|------------------------|-------------------------|--------------------------|--------------|-----------|
| Fossil taxa | | | | | | |
| <i>Pp. jonesi</i> | STS 565 | 47.3 | 114.3 | 77.3 | 0.6 | 12.6 |
| <i>Pp. broomi</i> | STS 544 | 53.8 | 179.8 | 98.3 | 0.5 | 9.7 |
| | MP 224 | 74.6 | 195.9 | 105.9 | 0.7 | 12.1 |
| | mean | 64.2 | 187.8 | 102.1 | 0.6 | 10.9 |
| <i>Pp. whitei</i> | MP 221 | 86.6 | 240.3 | 127.4 | 0.7 | 10.9 |
| <i>P. angusticeps</i> | KA 194 | 59.5 | 171.7 | 99.1 | 0.6 | 10.8 |
| <i>P. robinsoni</i> | SK 536 | 121.5 | 394.5 | 160.6 | 0.8 | 10.3 |
| | SK 555 | 139.0 | 475.6 | 191.1 | 0.7 | 9.3 |
| | SK 562 | 80.0 | 268.9 | 125.3 | 0.6 | 9.9 |
| | SK 602 | 109.5 | 339.1 | 151.5 | 0.7 | 10.4 |
| | mean | 115.5 | 366.8 | 156.0 | 0.7 | 10.3 |
| <i>Papio</i> sp. | Swartkrans 3 | 71.3 | 262.4 | 121.0 | 0.6 | 9.2 |
| <i>G. major</i> | KA 192 | 159.1 | 512.1 | 211.8 | 0.8 | 9.4 |
| | KA 193 | 106.9 | 481.0 | 183.1 | 0.6 | 7.4 |
| | | 133.0 | 497.6 | 197.5 | 0.7 | 8.4 |
| <i>T. o. oswaldi</i> | SK 561 | 221.7 | 649.2 | 270.9 | 0.8 | 9.5 |
| <i>T. o. darti</i> | MP 222 | 147.7 | 537.9 | 209.2 | 0.7 | 8.7 |
| <i>C. williamsi</i> | M 3055 | 36.7 | 142.2 | 75.1 | 0.5 | 9.4 |
| Extant taxa | | | | | | |
| <i>Papio</i> (n = 7) | mean | 63.2 | 210.4 | 103.1 | 0.6 | 10.3 |
| | range | 44.4–96.7 | 126.9–303.0 | 80.6–129.2 | 0.5–0.8 | 8.5–12.2 |
| <i>Theropithecus</i> (n = 2) | mean | 70.8 | 219.0 | 110.0 | 0.6 | 10.8 |
| | range | 63.2–78.4 | 180.7–257.3 | 95.8–124.2 | 0.6–0.7 | 9.9–11.7 |
| <i>Lophocebus</i> (n = 4) | mean | 16.5 | 45.0 | 39.2 | 0.4 | 11.7 |
| | range | 10.6–21.6 | 35.0–54.3 | 30.0–45.6 | 0.4–0.5 | 10.9–12.9 |
| <i>Mandrillus</i> (n = 2) | mean | 49.2 | 216.5 | 111.2 | 0.4 | 7.7 |
| | range | 35.9–62.5 | 139.2–293.7 | 79.2–143.1 | 0.4–0.5 | 6.6–8.7 |
| <i>Cercocebus</i> (n = 3) | mean | 33.1 | 92.1 | 68.2 | 0.5 | 10.6 |
| | range | 22.1–39.2 | 72.7–114.0 | 57.6–77.4 | 0.4–0.5 | 9.2–12.2 |
| <i>Macaca</i> (n = 3) | mean | 24.4 | 85.7 | 57.1 | 0.4 | 9.3 |
| | range | 9.3–35.2 | 43.3–113.5 | 29.9–74.8 | 0.3–0.5 | 8.8–9.7 |
| <i>Cercopithecus</i> (n = 1) | | 9.2 | 31.8 | 29.8 | 0.3 | 9.8 |
| <i>Erythrocebus</i> (n = 1) | | 16.8 | 66.8 | 51.4 | 0.3 | 8.0 |
| <i>Chlorocebus</i> (n = 4) | mean | 11.3 | 37.3 | 34.3 | 0.3 | 10.0 |
| | range | 9.1–12.8 | 26.1–42.3 | 25.8–39.0 | 0.3–0.4 | 8.0–11.9 |
| <i>Colobus</i> (n = 5) | mean | 15.0 | 48.3 | 38.6 | 0.4 | 10.8 |
| | range | 12.4–18.5 | 36.9–62.7 | 29.4–49.7 | – | 9.4–12.7 |
| <i>Ptilocolobus</i> (n = 1) | | 8.2 | 33.1 | 28.0 | 0.3 | 9.1 |

^a See text (Material and methods) for variable abbreviations.

Parapapio and *Gorgopithecus*) show higher 3D LAET than most species, with the exception of *Papio* and *Theropithecus gelada*. Values for *T. o. oswaldi* and *C. williamsi* lie near the upper and lower extremities of the Plio-Pleistocene species range, respectively. When compared to *Parapapio* and fossil *Papio*, the large *G. major*, *T. o. oswaldi* and *T. o. darti* fossil papionins display lower 3D LRET estimates.

The cartographies that map topographic enamel thickness variations at the outer UM3 crown surface of some extant and Plio-Pleistocene cercopithecoïd specimens are shown in Figure 4. In order to appreciate the differences in distribution, a scale ranging from zero to maximal values is proposed independently for each specimen. As anticipated by the LRET index, *Parapapio* and *P. angusticeps*, as well as the extant sample (excluding *Papio* and *Theropithecus*), display the thickest lateral enamel, especially along the lingual and the distal aspects. In contrast, *Papio robinsoni* shows localized areas of thick enamel mainly on the distal cusps, but also over the lingual side. This latter pattern of distribution is also found in extant *Papio* and *Theropithecus*, as well as in Plio-Pleistocene *Theropithecus*. The thin-enamelled condition seen in *C. williamsi* is close to the extant colobine pattern.

3.2. Enamel dentine junction morphology

The bgPCA analysis of EDJ shapes is shown in Figure 5 and the colour maps illustrating the changes from the GMS to each TMS are

depicted in Figure 1. The maximum value of the colour bar (1.5 mm) represents the highest amount of displacement recorded in our analysis. The bgPC1 axis discriminates the mesiodistally elongated and buccolingually contracted EDJ of fossil *Theropithecus*, also characterized by higher reliefs compared to the GMS. Similar morphological trends are observed in the TMS of living *Theropithecus*. However, the amount of displacement computed is lower compared to the fossil representatives. Therefore, the former are plotted closer to the rest of the sample in the bgPCA analysis (Fig. 5).

Parapapio and fossil *Papio* overlap and are near *Mandrillus*, extant *Papio* and *Macaca*. Overall, their EDJs fit well with the GMS but differ in their slightly higher cusps. In order to evaluate the variability within fossil papionins, we grouped fossil *Papio* and *Parapapio* to compute a TMS of their EDJs (Fig. 1) and assess the deviation from the TMS along the two first axes of the principal component computed on the GMS-to-individuals deformations (Fig. 2). According to the displacement maps, the distribution of the deformations among this group, as well as the magnitude, does not exceed the variability expressed by extant *Papio*.

Along bgPC1, *Gorgopithecus* is close to extant *Theropithecus* and *Mandrillus*, all showing a more contracted distal basin compared to the GMS. The only fossil colobine taxon included in our study, *C. williamsi*, plots in the positive values of the two axes, close to the colobines and *Chlorocebus*, *Erythrocebus* and *Cercopithecus*, and is

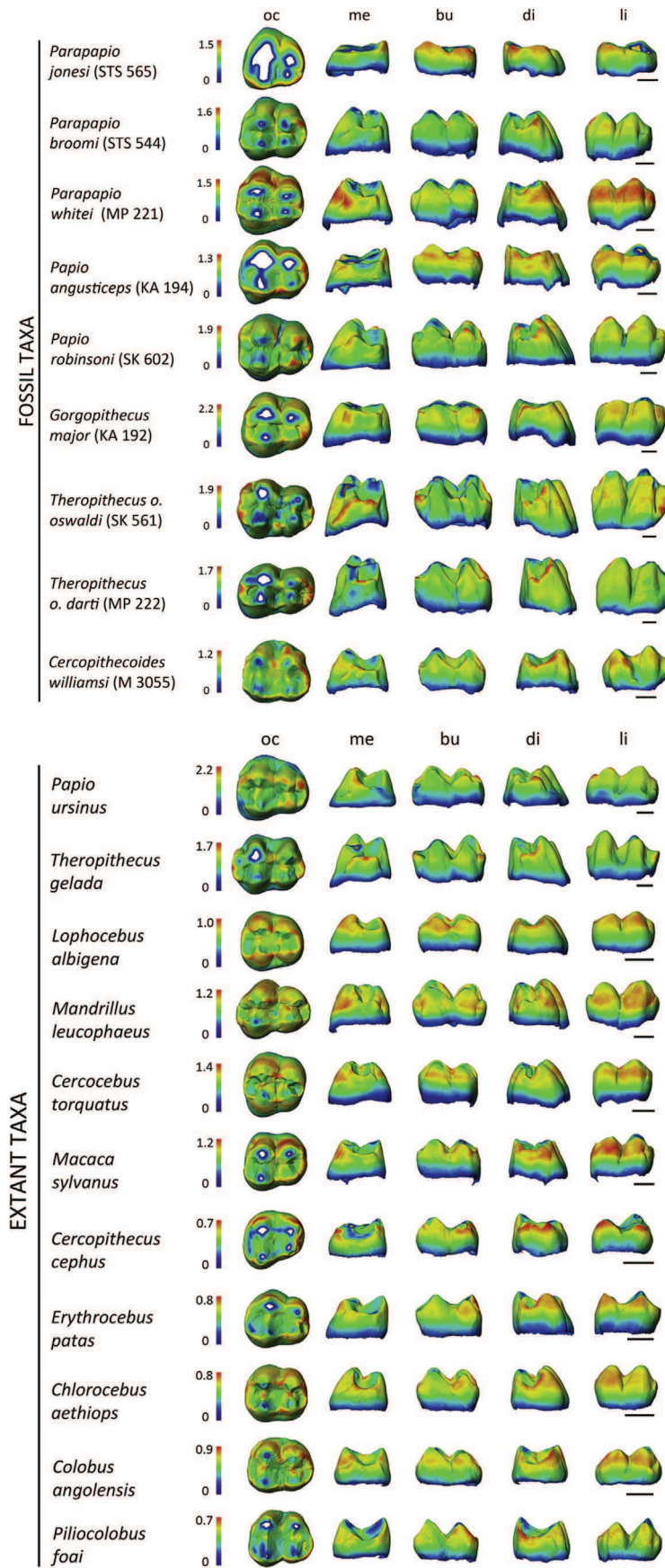


Figure 4. Enamel thickness cartographies of the upper third molar crown of some selected Plio-Pleistocene and extant cercopithecoïd specimens. Topographic thickness variation is rendered by a pseudo-colour scale ranging from thinner dark-blue to thicker red; isolated spots correspond to enamel removal following wear. Independently from their original side, all crowns are shown as right and imaged in occlusal (oc), mesial (me), buccal (bu), distal (di), and lingual (li) views. Because of significant variation in enamel thickness between species, a specific colour scale is attributed to each specimen (in mm). Scale bars: 3 mm. Data for STS 544, MP 221, STS 565, KA 194, SK 602, KA 192, M 3055 are from [Beaudet et al. \(2016\)](#).

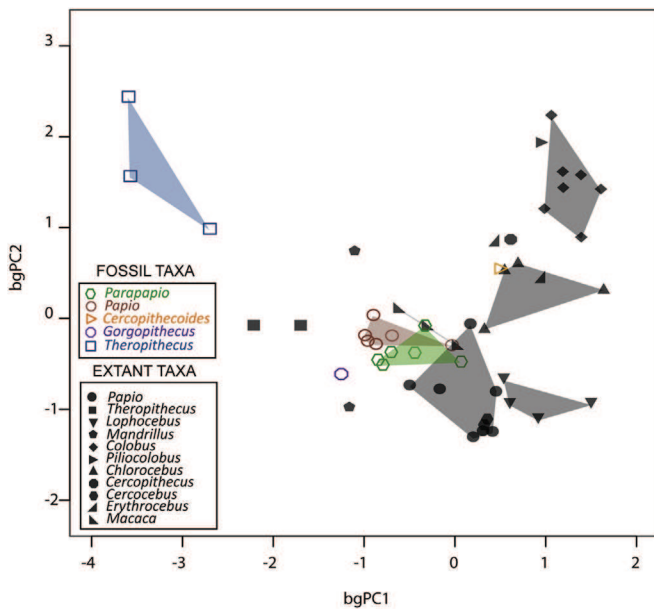


Figure 5. Between-group principal component analysis (bgPCA) of the deformation-based shape comparisons of the upper third molar enamel-dentine junctions in some Plio-Pleistocene and extant cercopithecooid specimens. Unfilled coloured symbols represent the fossil taxa. Shaded areas correspond to convex hulls.

characterized by marked relief on the lingual side and a particularly large distal basin compared to the GMS.

With regards to extant taxa, while overlapping along the first component, the bgPC2 axis better distinguishes the colobine taxa from the other extant monkeys because of higher distances between distal and mesial pairs of cusps in comparison to the GMS. As a consequence, the lengths of transverse crests and the areas of the basins are expanded. The *Lophochebus* specimens form a distinct group on the positive side of bgPC1, close to *Papio* and *Cercocebus*, and *Lophochebus* and *Cercocebus* are characterized by more reduced distal and mesial basins and lower cusps than the GMS. The *Erythrocebus* and *Cercopithecus* individuals are near the *Chlorocebus* group. These groups are defined by higher buccal crests and paracones compared to the global mean shape. Finally, relationships between taxa described by the CVA (Fig. 6) are similar to those observed with the bgPCA, except that in the former analysis the extinct *Papio* and *Parapapio* groups significantly overlap with extant *Papio* and *Macaca*.

For a better understanding of the distribution of morphological features in our sample, changes observed in the GMS-to-individuals deformations are synthesized through hierarchical clustering (HCPC) (Fig. 7). Seven groups (noted from “A” to “G”) are defined based on the level of the nodes. Primarily, the HCP discriminates the Colobini (group A) and Cercopithecini (group B) from the Papionini (*Papio*, *Macaca*, *Mandrillus*, *Theropithecus*, *Cercocebus* and *Lophochebus*). Most of the fossil specimens are included in groups E and F, together with *Mandrillus*, *Macaca*, and extant *Papio* specimens, with the notable exception of STS 251, included among the mangabeys (*Lophochebus* and *Cercocebus*, group C) and also *Theropithecus*. All members of this morpho-clade share an EDJ nearly undifferentiated from the global mean pattern, especially the fossil *Papio* and *Parapapio* specimens. The two *T. o. darti* (group D) specimens form an isolated group whereas the second Plio-Pleistocene *Theropithecus* taxon included in our study (*T. o. oswaldi*) is morphologically closer to *T. gelada* (group G). We observe that the EDJ shape distinguishes the mangabeys (group C) from the other papionins.

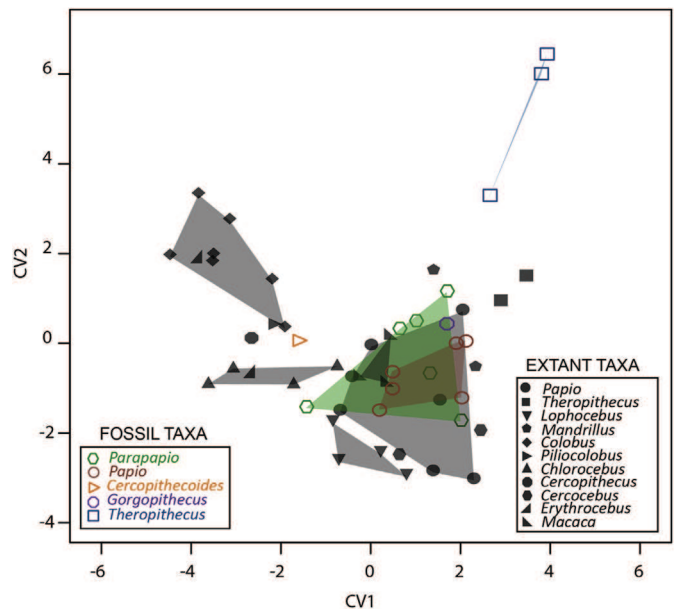


Figure 6. Canonical variate analysis (CVA) of the deformation-based shape comparisons of the upper third molar enamel-dentine junctions in some Plio-Pleistocene and extant cercopithecooid specimens. Unfilled coloured symbols represent the fossil taxa. Shaded areas correspond to convex hulls.

3.3. Semicircular canal morphology

We first computed a bgPCA on the bony labyrinth Procrustes shape coordinates (Fig. 8). While extant *Theropithecus*, *Piliocolobus*, and *Dinopithecus* are reasonably discriminated from the rest of the sample, most of the taxa overlap. Given that the SCC morphology described in our sample does not clearly distinguish the genera represented in our sample, we further explored the relationship between groups by performing a CVA as shown in Figure 9A and 9B (for the three first components). The shapes at the extremities of the two axes illustrate the morphological variation trends along each component. The two *D. ingens* specimens fall very close to each other and approximate the extant *Macaca* distribution in the positive values of CV1, corresponding to a twisted lateral canal. Modern *Theropithecus* is set apart in the negative space of CV2 because of a larger diameter for the posterior semicircular canal, as compared to the other groups. While the *Cercopithecooides* individuals approximate the condition of extant *Colobus* and *Chlorocebus* along the three axes, the fossil *Theropithecus* specimens are found between the extant groups without any clear trend. Among the extant sample, the *Mandrillus* estimate nears the *Cercocebus* one along the three axes whereas *Lophochebus* approximates the extant *Papio* variability in the negative space of CV1.

According to the loadings computed from the CVA and rendered by a colour scale onto the semilandmarks (Fig. 9C), the SCC areas that mostly contribute to the variability observed along the three axes are located around changes in slope on the posterior canal and near the intersections of the canals with the common crus.

3.4. Comparing signals from the enamel-dentine junction and the semicircular canals

The comparison of the taxonomic signals extracted from the EDJ and the SCC was achieved through the selection of specimens that preserved both the third molar and the bony labyrinth (a total of 40 specimens, including six fossils). We performed a bgPCA and a CVA

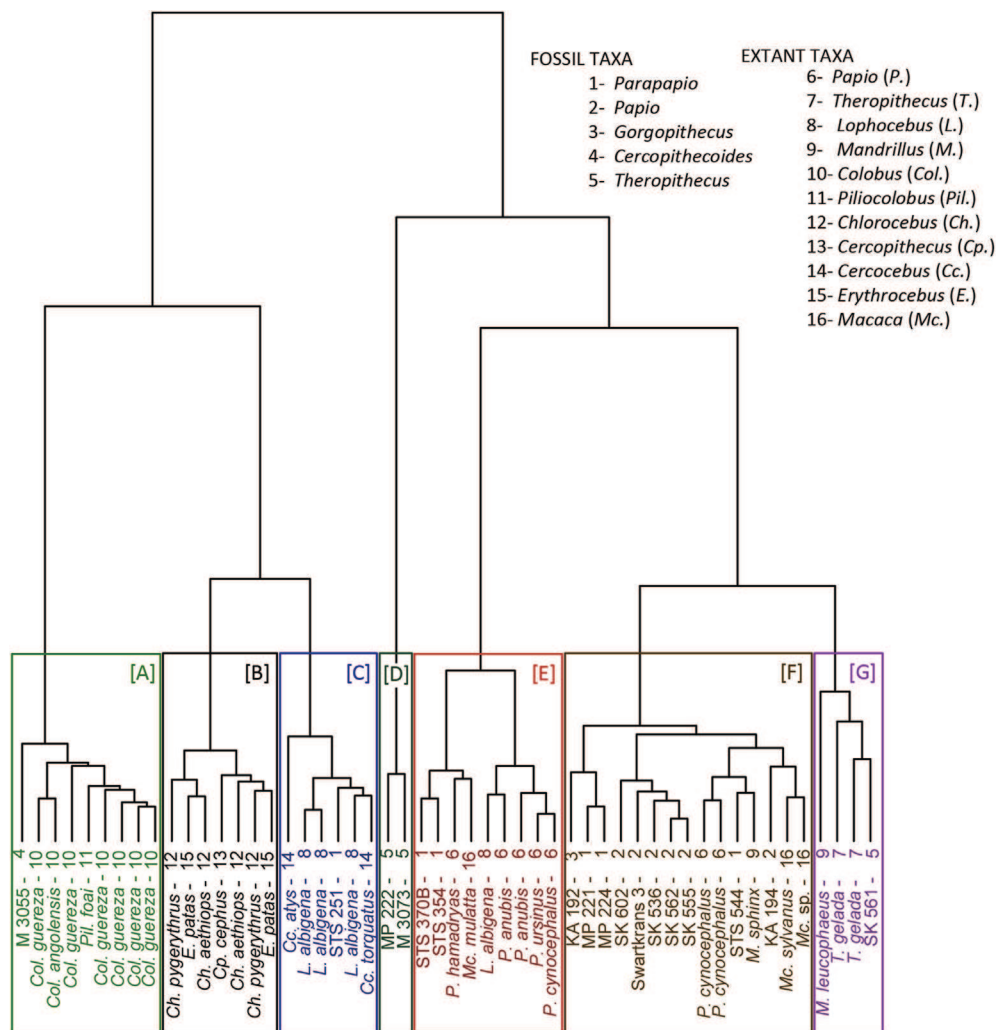


Figure 7. Hierarchical classification based on the distances computed from the deformation process of the upper third molar enamel-dentine junctions (GMS-to-individuals) in some Plio-Pleistocene and extant cercopithecoid specimens. The genus sampled at each terminal branch is coded by one number (listed above).

for each structure and directly compared the results (Fig. 10A–D). On the whole, the interpretations in terms of affinities between genera are consistent between the two structures. Concerning the fossil specimens, *Cercopithecoides* plots close to *Chlorocebus* whereas *Parapapio* plots near the extant *Papio* group. Extinct and extant *Theropithecus* species are discriminated from the rest of the sample in all the four analyses, especially for teeth. The two *Mandrillus* individuals are found close to the *Theropithecus* specimens. In contrast, there is no distinct pattern in other papionin genera and *Lophocebus*, *Cercocebus*, *Macaca* and *Papio* cluster in most of the analyses. Finally, unlike with SCC morphology, the colobines *Ptilocolobus* and *Colobus* are grouped together when EDJ shape is considered.

4. Discussion and conclusions

The use of virtual imaging in this study of extant and Plio-Pleistocene cercopithecoids brings fresh data to help understand fossil morphological variability and discrimination of taxa. Previous studies have demonstrated the utility of noninvasive imaging methods for the taxonomic assignment of isolated cercopithecoid remains (Beaudet, 2015; Beaudet et al., 2015, 2016). To the best of our knowledge, our current study represents the first combined 3D

virtual analyses of molar tissue proportions, EDJ morphology and inner ear shape in Plio-Pleistocene cercopithecoid assemblages.

4.1. Enamel thickness and enamel-dentine junction morphology

Previous bidimensional (2D) studies based on natural, histological, or virtual sections of lower permanent molars have revealed thick enamel for the papionins *Lophocebus*, *Cercocebus*, *Papio* and *Mandrillus* in comparison with *Colobus* and the cercopithecins *Cercopithecus*, *Chlorocebus* and *Erythrocebus* (Kay, 1981; Shellis et al., 1998), a pattern supported by our analyses. While distinct mean values of relative enamel thickness were recorded for *Lophocebus* and *Cercocebus* by Dumont (1995), in our study the two groups differ mainly in terms of variability (see ranges in Table 2). Our measurements of RET in molars are consistent with the results published by Olejniczak et al. (2008c) for *Cercocebus* (mean 17.6) but not for *Macaca* (mean 13.7) and *Papio* (mean 14.8), nor with those of extant macaques investigated by Kato et al. (2014) (mean 12.2–14.1). Regarding specifically the enamel thickness recorded for *Papio*, our estimates for both AET and RET are in accordance with ranges proposed by Grine et al. (2005) and Hlusko et al. (2004).

Relative enamel thickness (RET) values for extant papionins indicate an “intermediate/thick” enamel condition (sensu Martin,

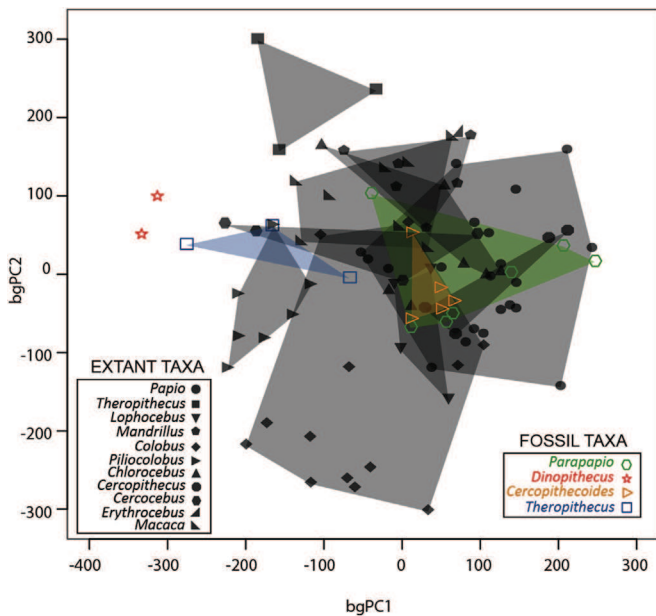


Figure 8. Between-group principal component analysis (bgPCA) of the Procrustes-registered shape coordinates of the bony labyrinth morphology computed for some Plio-Pleistocene and extant cercopithecoïd specimens. Unfilled coloured symbols represent the fossil taxa. Shaded areas correspond to convex hulls.

1985). However, we observe that, on the whole, fossil cercopithecoïds fit more confidently in the “intermediate/thin” enamel category. In comparison with large Plio-Pleistocene papionins *G. major*, *T. o. oswaldi*, *T. o. darti* and with the colobine *C. williamsi*, the scale-free LRET measured in fossil *Papio* and *Parapapio* is globally thicker. The adaptive significance of thick or thin enamel and the dietary assessments from enamel thickness values are unclear. However, it is noteworthy that significant differences in diet (more specifically in the proportion of C_4 -based resources intake) between Plio-Pleistocene and extant South African cercopithecoïds were described by isotopic and microwear analyses (Codron et al., 2005; El-Zaatari et al., 2005).

In agreement with the established classification of cercopithecoïd primates (Szalay and Delson, 1979; Strasser and Delson, 1987; Fleagle, 2013), EDJ shapes discriminate the three tribes Colobini, Cercopithecini and Papionini (Fig. 7). The inclusion of *C. williamsi* among the colobines and its separation from the rest of the contemporaneous cercopithecoïd taxa suggests specific features for this species shared with extant colobine representatives (Szalay and Delson, 1979). Our structural investigation of the internal UM3 in fossil *Theropithecus* confirms its high degree of specialization in EDJ morphology (sensu Jablonski, 1993; Jablonski and Frost, 2010), already suggested from outer occlusal morphology (Jolly, 1972; Szalay and Delson, 1979; Jablonski, 1993). Also, in our analyses, the large-bodied papionin *G. major* shows some similarities with extant and fossil *Theropithecus* in terms of enamel thickness and dental morphology, which may be interesting given a previous suggestion of phylogenetic affinities (Folinsbee, 2008; but see Gilbert, 2013). In accordance with external dental morphology (e.g., Freedman, 1957), the characterization of the morphostructural variations of the EDJ did not help to distinguish *Parapapio* from fossil *Papio* (Fig. 2) based on our current limited sample. The tentative interest of these features for the diagnosis of *Papio* and *Parapapio* may be supported or rejected only by enlarging both the extant and extinct samples.

Fossil *Papio* and *Parapapio* specimens share with *Macaca* an EDJ nearly undifferentiated from the global mean pattern.

Because *Macaca* is largely accepted as the sister taxon of the African papionins representing the ancestral morphotype (Delson, 1975), it could be hypothesized that the Plio-Pleistocene species of *Papio* and *Parapapio* were morphologically close to the ancestor shared with *Macaca*, and that *Mandrillus* and extant *Papio* (within the limits of our sample) retain the ancestral pattern. Moreover, it is significant that Gilbert (2013), in his phylogenetic studies of Plio-Pleistocene and extant papionins, found a crown group including *Papio hamadryas*, *G. major* and *Papio angusticeps* and suggested that this cluster constitutes a group of generalists. In contrast, the mangabeys and *Theropithecus* are derived compared to this ancestral pattern. Consequently, our preliminary analyses suggest that EDJ shape could be especially informative for discriminating and tracking the phylogenetic position of highly autapomorphic taxa such as *Theropithecus*. Similarities found in the EDJ morphology between *Lophocebus* and *Cercocebus* may be interpreted as parallel evolution from the ancestral condition. However, further analyses including a significantly larger mangabey sample are needed to investigate this hypothesis more finely.

The combination of statistical analysis of morphometric and volumetric variables has the potential to aid in discriminating taxa. In our study we illustrate the potential benefit of hierarchical clustering (HCPC) compared to classical component analyses (bgPCA, CVA) limited to two dimensions only (i.e., two components). More specifically, through this exploratory analysis the position of some particular specimens could be described and approaches proposed for future studies. For instance, based on the HCPC (Fig. 7), the fossil *Theropithecus* subspecies were separately classified, which potentially suggests distinct morphological affinities; this needs to be tested with additional specimens. The possibility of distinguishing the two *T. oswaldi* subspecies, *T. o. oswaldi* and *T. o. darti*, based on EDJ morphology may be very valuable, especially because of the potential of dental features in the search for time-sensitive biological structures among the lineage (Jolly, 1972; Frost and Delson, 2002; Gilbert et al., 2014). Also, it is noteworthy that the *Parapapio* specimen from Sterkfontein Member 4 (STS 251) is included among the mangabeys, given that dental affinities between papionins from Sterkfontein and extant *Lophocebus* have previously been mentioned (Heaton, 2006).

For direct comparisons of UM3 with other molars, the question of metameric variation in enamel thickness should be addressed in future studies, particularly because significant metameric variation was detected in extant baboon molar enamel (Hlusko et al., 2004). Moreover, by analysing 2D sections of *Papio ursinus* maxillary molars, Olejniczak et al. (2007) demonstrated that EDJ morphology varies along the molar row.

4.2. Semicircular canal morphology

Unlike the EDJ, inner ear morphology in *Cercocebus* specimens is closer to *Mandrillus* than to *Lophocebus*. Since molecular studies have consistently demonstrated a monophyletic *Cercocebus* and *Mandrillus* group (Disotell, 2000; Harris, 2000; Tosi et al., 2003), we can hypothesize that other affinities between taxa revealed by our SCC analyses are phylogenetically informative. Through the SCC analyses, extant *Theropithecus* was discriminated from the rest of the sample, suggesting a diagnostic pattern for this feature even if our analysis is, for now, limited to three individuals. The SCC morphology described in the large *D. ingens* differs from that of any other fossil specimens represented in our sample. Our study of one adult male (SK 599) and one juvenile female (SK 554) suggests that our criteria may be considered as appropriate to investigate taxonomic affinities, independent of sex attribution or developmental

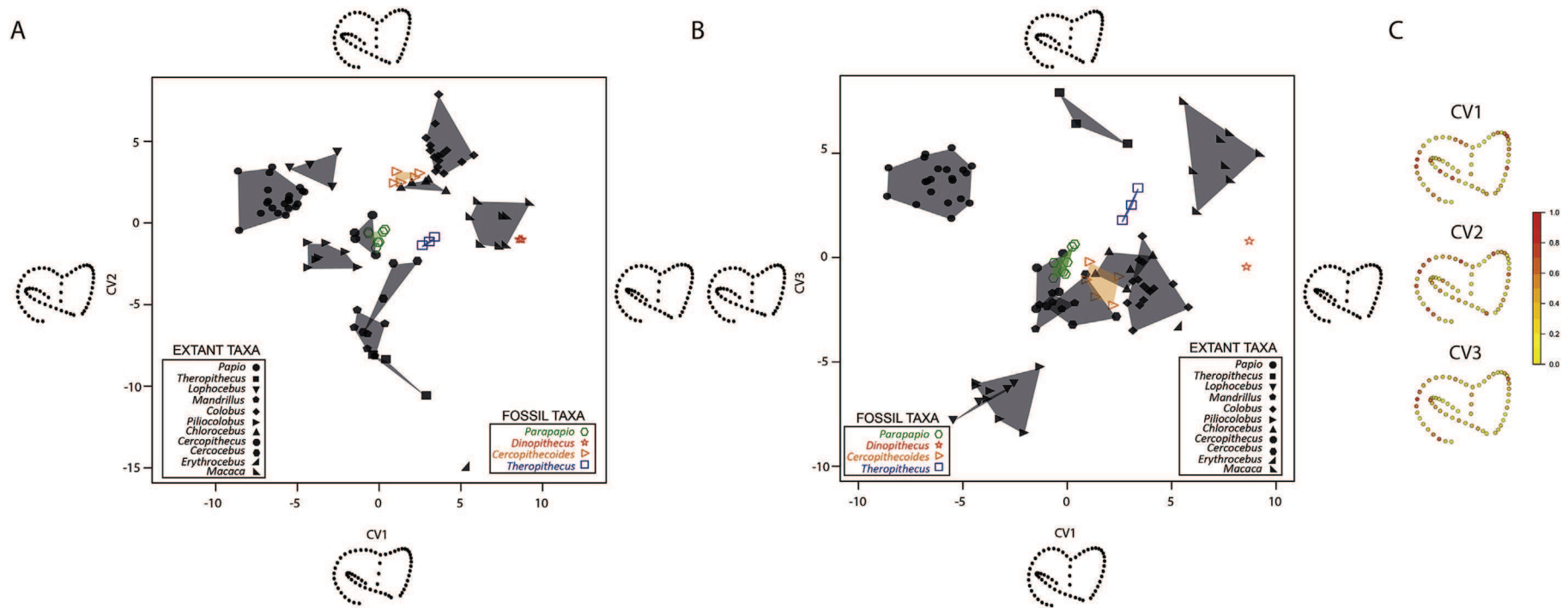


Figure 9. Canonical variate analysis (CVA) of the Procrustes-registered shape coordinates of the bony labyrinth morphology calculated for some Plio-Pleistocene and extant cercopithecoïd specimens and computed for the components CV1 and CV2 (A) and CV1 and CV3 (B). The shapes at the extremities of the axes illustrate the morphological variation trends along each component. Contributions of the semilandmarks to the total variance observed (standardized loadings) along each component are rendered by a colour scale (C). Unfilled coloured symbols represent the fossil taxa. Shaded areas correspond to convex hulls.

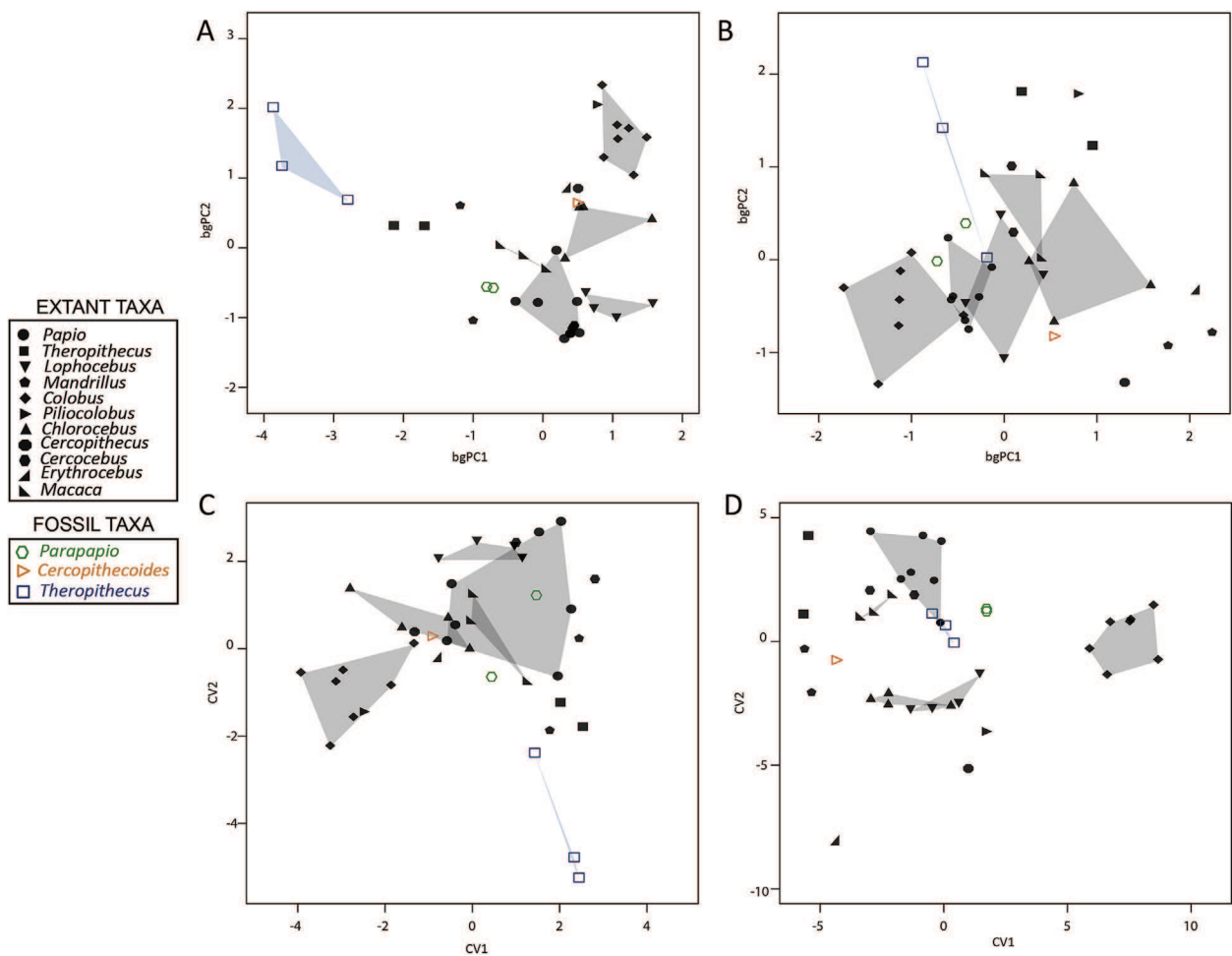


Figure 10. Between-group principal component analysis (bgPCA) and canonical variate analysis (CVA) of the deformation-based shape comparisons of the upper third molar enamel-dentine junctions (bgPCA: A; CVA: C) and of the Procrustes-registered shape coordinates of the bony labyrinth morphology (bgPCA: B; CVA: D) in selected Plio-Pleistocene and extant cercopithecoïd specimens that preserve both structures. Unfilled coloured symbols represent the fossil taxa. Shaded areas correspond to convex hulls.

stage (Freedman, 1957). However, given the large size estimated for *Dinopithecus*, a potential allometric influence cannot be discounted pending further analyses.

Spoor and Zonneveld (1998), by investigating the inner ear morphology of extant cercopithecoïds as part of their comparative sample for the characterization of the human condition, revealed similarities between human labyrinthine morphology and that of large cercopithecoïds. In this context, homoplasy was suggested to be responsible for these similarities, and *Macaca* was proposed to represent the ancestral labyrinthine morphology of the anthropoids, and probably all primates (shared with hylobatids, ateloids and prosimians). Interestingly, the condition displayed by *Dinopithecus* approximates that of *Macaca*, potentially suggesting the retention of a primitive state of the inner ear that is not shared with contemporaneous fossil taxa.

On the whole, variations of SCC shape are not demonstrated here as efficient diagnostic features for extinct cercopithecoïd taxa using classical discriminant analyses (Fig. 8), but they are informative for the detection of morphological affinities (Fig. 9). These results could likely be explained by the combination of functional signals, influenced by locomotor behaviour. Because agility and head movements were proved to influence semi-circular canal configurations (Spoor et al., 2002; Malinjak et al., 2012), and given that cercopithecoïd taxa (both extant and extinct) considered in this study are mainly semi-terrestrial

(Jablonski and Frost, 2010; Fleagle, 2013), the relative homogeneity described for the inner ear could be due to the lack of locomotor diversity.

4.3. Combined use of craniodental internal structures

By directly comparing taxonomic signals extracted from the EDJ and the SCC of the same individuals, our analysis suggests the value of combining various internal structures. The consistency of our analyses tends to suggest that these two structures could be independently considered for taxonomic studies and provide convergent conclusions. However, the pattern displayed by the variations of EDJ shape is closer to the current taxonomy, notably by grouping the colobines together. One intriguing result that should be explored in the future is the proximity of *C. williamsi* to the guenon *Chlorocebus*. Also, further analyses focussing on papionin taxa would be valuable for the understanding of morphological affinities within this tribe, as they were not clearly discriminated in our study.

Acknowledgements

We are indebted to S. Potze (Pretoria), B. Zipfel (Johannesburg), J. Cuisin (Paris), G. Fleury (Toulouse), E. Gilissen and W. Wendelen (Tervuren) for having granted access to fossil and comparative

material under their care. We also thank K. Carlson and T. Jashashvili (Johannesburg), G. Clément and M. Garcia-Sanz (Paris) for microtomographic acquisitions and E. Delson (New York) for providing CT scans. For scientific contribution and/or for discussion and comments on the results presented in this study, we are especially grateful to E. Delson (New York), S. Durrleman (Paris), S. Elton (Durham), D. Ginibriere (Toulouse), J. Heaton (Birmingham), L. Hlusko (Berkeley), N. Jablonski (University Park), O. Kullmer (Frankfurt), R. Macchiarelli (Poitiers and Paris), M. Nakatsukasa (Kyoto), L. Pan (Toulouse), C. Zanolli (Pretoria and Toulouse). The present version greatly benefited from the comments provided by the Editor, the Associate Editor and three anonymous reviewers. The French research federation FERMA_T (FR3089), the National Research Foundation (NRF) and Department of Science and Technology (DST) of South Africa are acknowledged for providing micro-X-ray tomography laboratory facility. This project was granted access to the HPC resources of CALMIP supercomputing centre under the allocation 2015-[P1440] attributed to the laboratory AMIS. Research supported by the Centre of Research and Higher Education (PRES) of Toulouse, the Midi-Pyrénées Region and the French Ministry of Foreign Affairs.

References

- Bayle, P., Bondioli, L., Macchiarelli, R., Mazurier, A., Puyménil, L., Volpato, V., Zanolli, C., 2011. Three-dimensional imaging and quantitative characterization of human fossil remains. Examples from the NESPOS database. In: Macchiarelli, R., Weniger, G.C. (Eds.), *Pleistocene Databases. Acquisition, Storing, Sharing*. Wissenschaftliche Schriften des Neanderthal Museums 4, Mettmann, pp. 29–46.
- Beaudet, A., 2015. Caractérisation des structures crâniennes internes des cercopithecoides et étude diachronique de leurs variations morphologiques dans la séquence Plio-Pleistocène sud-africaine. Ph.D. Dissertation, Université de Toulouse.
- Beaudet, A., Zanolli, C., Engda Redae, B., Endalamaw, M., Braga, J., Macchiarelli, R., 2015. A new cercopithecoid dentognathic specimen attributed to *Theropithecus* from the late Early Pleistocene (c. 1 Ma) deposits of Simbiro, at Melka Kunture, Ethiopian highlands. *Palevol* 14, 657–669.
- Beaudet, A., Braga, J., de Beer, F., Schillinger, B., Steininger, C., Vodopivec, V., Zanolli, C., 2016. Neutron microtomography-based virtual extraction and analysis of a cercopithecoid partial cranium (STS 1039) embedded in a breccia fragment from Sterkfontein Member 4 (South Africa). *Am. J. Phys. Anthropol.* 159, 737–745.
- Benazzi, S., Fornai, C., Bayle, P., Coquerelle, M., Kullmer, O., Mallegni, F., Weber, G.W., 2011. Comparison of dental measurement systems for taxonomic assignment of Neanderthal and modern human lower second deciduous molars. *J. Hum. Evol.* 61, 320–326.
- Bettridge, C.M., Dunbar, R.I.M., 2012. Modeling the biogeography of fossil baboons. *Int. J. Primatol.* 33, 1278–1308.
- Bondioli, L., Bayle, P., Dean, C., Mazurier, A., Puyménil, L., Ruff, C., Stock, J.T., Volpato, V., Zanolli, C., Macchiarelli, R., 2010. Morphometric maps of long bone shafts and dental roots for imaging topographic thickness variation. *Am. J. Phys. Anthropol.* 142, 328–334.
- Bookstein, F.L., 1991. *Morphometric Tools for Landmark Data: Geometry and Biology*. Cambridge University Press, Cambridge.
- Braga, J., Thackeray, J.F., Dumoncel, J., Descouens, D., Bruxelles, L., Loubes, J.-M., Kahn, J.-L., Stambanoni, M., Bam, L., Hoffman, J., de Beer, F., Spoor, F., 2013. A new partial temporal bone of a juvenile hominin from the site of Kromdraai B (South Africa). *J. Hum. Evol.* 65, 447–456.
- Braga, J., Loubes, J.-M., Descouens, D., Dumoncel, J., Thackeray, J.F., Kahn, J.-L., de Beer, F., Riberon, A., Hoffman, K., Balaesque, P., Gilissen, E., 2015. Disproportionate cochlear length in genus *Homo* shows a high phylogenetic signal during apes' hearing evolution. *PLOS ONE* 10 (6), e0127780. <http://dx.doi.org/10.1371/journal.pone.0127780>.
- Brain, C.K., 1981. *The Hunters or the Hunted? An Introduction to African Cave Taphonomy*. University of Chicago Press, Chicago.
- Broom, R., 1940. The South African Pleistocene cercopithecoid apes. *Ann. Transv. Mus.* 20, 89–100.
- Codron, D., Luyt, J., Lee-Thorp, J.A., Sponheimer, M., de Ruiter, D., Codron, J., 2005. Utilization of savanna-based resources by Plio-Pleistocene baboons. *S. Afr. J. Sci.* 101, 245–248.
- Dechow, P.C., Singer, R., 1984. Additional fossil *Theropithecus* from Hopefield, South Africa: a comparison with other African sites and a reevaluation of its taxonomic status. *Am. J. Phys. Anthropol.* 63, 405–435.
- Delson, E., 1973. Fossil colobine monkeys of the Circum-Mediterranean region and the evolutionary history of the Cercopithecidae (Primates, Mammalia). Ph.D. Dissertation, Columbia University.
- Delson, E., 1975. Evolutionary history of the Cercopithecidae. In: Szalay, F.S. (Ed.), *Approaches to Primate Paleobiology, Contributions to Primatology* 4. Karger, Basel, pp. 167–217.
- Delson, E., 1984. Cercopithecoid biochronology of the African Plio-Pleistocene: correlation among eastern and southern hominid-bearing localities. *Cour. Forsch. Inst. Senckenberg* 69, 199–218.
- Delson, E., 1988. Chronology of South African australopithecids site units. In: Grine, F.E. (Ed.), *Evolutionary History of the 'Robust' Australopithecines*. Aldine de Gruyter, New York, pp. 317–324.
- Delson, E., Dean, D., 1993. Are *Papio baringensis* R. Leakey, 1969, and *P. quadratiostris* Iwamoto, 1982, species of *Papio* or *Theropithecus*? In: Jablonski, N.G. (Ed.), *Theropithecus: the Rise and Fall of a Primate Genus*. Cambridge University Press, Cambridge, pp. 157–189.
- Disotell, T.R., 2000. Molecular systematics of the Cercopithecidae. In: Whitehead, P.F., Jolly, C.J. (Eds.), *Old World Monkeys*. Cambridge University Press, Cambridge, pp. 29–56.
- Dumoncel, J., Durrleman, S., Braga, J., Jessel, J.-P., Subsol, G., 2014. Landmark-free 3D method for comparison of fossil hominins and hominids based on endocranium and EDJ shapes. *Am. J. Phys. Anthropol.* 153, 110.
- Dumont, E.R., 1995. Enamel thickness and dietary adaptation among extant primates and chiropterans. *J. Mammal.* 76, 1127–1136.
- Durrleman, S., 2010. Statistical models of currents for measuring the variability of anatomical curves, surfaces and their evolution. Ph.D. Dissertation, University of Nice-Sophia Antipolis.
- Durrleman, S., Pennec, X., Trouvé, A., Ayache, N., Braga, J., 2012a. Comparison of the endocranial ontogenies between chimpanzees and bonobos via temporal regression and spatiotemporal registration. *J. Hum. Evol.* 62, 74–88.
- Durrleman, S., Prastawa, M., Korenberg, J.R., Joshi, S., Trouvé, A., Gerig, G., 2012b. Topology preserving atlas construction from shape data without correspondence using sparse parameters. In: Ayache, N., Delingette, H., Golland, P., Mori, K. (Eds.), *Proceedings of Medical Image Computing and Computer Aided Intervention*. Nice, France, pp. 223–230.
- Durrleman, S., Prastawa, M., Charon, N., Korenberg, J.R., Joshi, S., Gerig, G., Trouvé, A., 2014. Morphometry of anatomical shape complexes with dense deformations and sparse parameters. *NeuroImage* 101, 35–49.
- Eisenhart, W.L., 1974. The fossil cercopithecoids of Makapansgat and Sterkfontein. A.B. Thesis, Harvard College.
- El Zaatari, S., Grine, F.E., Teaford, M.F., Smith, H.F., 2005. Molar microwear and dietary reconstruction of fossil Cercopithecoida from the Plio-Pleistocene deposits of South Africa. *J. Hum. Evol.* 49, 180–205.
- Elton, S., 2001. Locomotor and habitat classification of cercopithecoid postcranial material from Sterkfontein Member 4, Bolt's Farm and Swartkrans Members 1 and 2, South Africa. *Palaeont. Afr.* 37, 115–126.
- Elton, S., 2006. Forty years on and still going strong: the use of hominin-cercopithecoid comparisons in paleoanthropology. *J. R. Anthropol. Inst.* 12, 19–38.
- Elton, S., Bishop, L.C., Wood, B., 2001. Comparative context of Plio-Pleistocene hominin brain evolution. *J. Hum. Evol.* 41, 1–27.
- Fleagle, J.G., 2013. *Primate Adaptation and Evolution*. Academic Press, New York.
- Folinsbee, K.E., 2008. Evolutionary history and biogeography of papionin monkeys. Ph.D. Dissertation, University of Toronto.
- Fourie, N.H., Lee-Thorp, J.A., Ackermann, R.R., 2008. Biogeochemical and cranio-metric investigation of dietary ecology, niche separation, and taxonomy of Plio-Pleistocene cercopithecoids from the Makapansgat Limeworks. *Am. J. Phys. Anthropol.* 135, 121–135.
- Freedman, L., 1957. The fossil Cercopithecoida of South Africa. *Ann. Transv. Mus.* 23, 121–262.
- Freedman, L., 1976. South African fossil Cercopithecoida: a re-assessment including a description of new material from Makapansgat, Sterkfontein and Taung. *J. Hum. Evol.* 5, 297–315.
- Freedman, L., Brain, C.K., 1977. A re-examination of the cercopithecoid fossils from Swartkrans (Mammalia: Cercopithecidae). *Ann. Transv. Mus.* 30, 211–218.
- Frost, S.R., 2001. Fossil Cercopithecidae of the Afar depression, Ethiopia: species systematics and comparison to the Turkana Basin. Ph.D. Dissertation, The City University of New York.
- Frost, S.R., 2007. Fossil Cercopithecidae from the Middle Pleistocene Dawaitoli Formation, Middle Awash Valley, Afar Region, Ethiopia. *Am. J. Phys. Anthropol.* 134, 460–471.
- Frost, S.R., Delson, E., 2002. Fossil Cercopithecidae from the Hadar Formation and surrounding areas of the Afar Depression, Ethiopia. *J. Hum. Evol.* 43, 687–748.
- Gantt, D.G., 1977. Enamel of primate teeth: its structure with reference to functional and phyletic implications. Ph.D. Dissertation, Washington University.
- Gilbert, C.C., 2007a. Craniomandibular morphology supporting the diphyletic origin of mangabeys and a new genus of the *Cercocebus/Mandrillus* clade, *Procercocebus*. *J. Hum. Evol.* 53, 69–102.
- Gilbert, C.C., 2007b. Identification and description of the first *Theropithecus* (Primates: Cercopithecidae) material from Bolt's Farm, South Africa. *Ann. Transv. Mus.* 44, 1–10.
- Gilbert, C.C., 2008. African papionin phylogenetic history and Plio-Pleistocene biogeography. Ph.D. Dissertation, Stony Brook University.
- Gilbert, C.C., 2013. Cladistic analysis of extant and fossil African papionins using craniodental data. *J. Hum. Evol.* 64, 399–433.
- Gilbert, C.C., Frost, S.R., Delson, E., 2013. Appearance of the modern baboon, *Papio hamadryas*, in the Plio-Pleistocene fossil record: Evidence from South Africa. *Am. J. Phys. Anthropol.* 129.

- Gilbert, C.C., Frost, S.R., Delson, E., 2014. African Plio-Pleistocene biochronology: a reassessment using cercopithecoïd taxa. *Am. J. Phys. Anthropol.* 153, 124.
- Gilbert, C.C., Steininger, C.M., Kibii, J.M., Berger, L.R., 2015. *Papio* cranium from the hominin-bearing site of Malapa: implications for the evolution of modern baboon cranial morphology and South African Plio-Pleistocene biochronology. *PLOS ONE* 10, e0133361. <http://dx.doi.org/10.1371/journal.pone.0133361>.
- Gilbert, C.C., Frost, S.R., Delson, E., 2016. Reassessment of Olduvai Bed 1 cercopithecoïds: A new biochronological and biogeographical link to the South African fossil record. *J. Hum. Evol.* 92 (Suppl 54), 50–59.
- Gittins, R., 1985. *Canonical Analysis: A Review with Applications in Ecology*. Springer-Verlag, Berlin.
- Glaunès, J.A., Joshi, S., 2006. Template estimation from unlabeled point set data and surfaces for computational anatomy. In: Pennec, X., Joshi, S. (Eds.), *Proceedings of the International Workshop on the Mathematical Foundations of Computational Anatomy*. Copenhagen, Denmark, pp. 29–39.
- Grine, F.E., Spencer, M.A., Demes, B., Smith, H.F., Strait, D.S., Constant, D.A., 2005. Molar enamel thickness in the chacma baboon, *Papio ursinus* (Kerr 1792). *Am. J. Phys. Anthropol.* 128, 812–822.
- Gunz, P., Ramsier, M., Kuhrig, M., Hublin, J.-J., Spoor, F., 2012. The mammalian bony labyrinth reconsidered, introducing a comprehensive geometric morphometric approach. *J. Anat.* 220, 529–543.
- Harris, E.E., 2000. Molecular systematics of the Old World monkey tribe Papionini: analysis of the total available genetic sequences. *J. Hum. Evol.* 38, 235–256.
- Hartwig, W., 2002. *The Primate Fossil Record*. Cambridge University Press, Cambridge.
- Heaton, J.L., 2006. Taxonomy of the Sterkfontein fossil Cercopithecoïdinae: the Papionini of Members 2 and 4 (Gauteng, South Africa). Ph.D. Dissertation, Indiana University.
- Hlusko, L.J., Suwa, G., Kono, R.T., Mahaney, M.C., 2004. Genetics and the evolution of primate enamel thickness: a baboon model. *Am. J. Phys. Anthropol.* 124, 223–233.
- Hoffman, J.W., de Beer, F.C., 2012. Characteristics of the micro-focus X-ray tomography facility (MIXRAD) at Ncsa in South Africa. In: 18th World Conference of Nondestructive Testing, Durban, South Africa.
- Jablonski, N.G., 1993. *Theropithecus: The Rise and Fall of a Primate Genus*. Cambridge University Press, Cambridge.
- Jablonski, N.G., 2002. Fossil Old World monkeys: the late Neogene radiation. In: Hartwig, W.C. (Ed.), *The Primate Fossil Record*. Cambridge University Press, Cambridge, pp. 255–299.
- Jablonski, N.G., Frost, S., 2010. Cercopithecoïdeia. In: Werdelin, L., Sanders, W.J. (Eds.), *Cenozoic Mammals of Africa*. University of California Press, Berkeley, pp. 393–428.
- Jolly, C.J., 1970. The seed eaters: a new model of hominid differentiation based on a baboon analogy. *Man* 5, 5–26.
- Jolly, C.J., 1972. The classification and natural history of *Theropithecus* (*Simopithecus*) (Andrews, 1916), baboons of the African Plio-Pleistocene. *Bull. Br. Mus. Nat. Hist. Geol.* 22, 1–122.
- Jolly, C.J., 2001. A proper study for mankind: analogies from the papionin monkeys and their implications for human evolution. *Yearb. Phys. Anthropol.* 44, 177–204.
- Kato, A., Tang, N., Borries, C., Papakyriakos, A.M., Hinde, K., Miller, E., Kunitatsu, Y., Hirasaki, E., Shimizu, D., Smith, T.M., 2014. Intra- and interspecific variation in macaque molar enamel thickness. *Am. J. Phys. Anthropol.* 155, 447–459.
- Kay, R.F., 1981. The nut-crackers—a new theory of the adaptations of the Ramapithecoïdinae. *Am. J. Phys. Anthropol.* 55, 141–151.
- Kirk, E.C., Gosselin-Ildari, A.D., 2009. Cochlear labyrinth volume and hearing abilities in primates. *Anat. Rec.* 292, 765–776.
- Kono, R., 2004. Molar enamel thickness and distribution patterns in extant great apes and humans: new insights based on a 3-dimensional whole crown perspective. *Anthropol. Sci.* 112, 121–146.
- Lê, S., Josse, J., Husson, F., 2008. FactoMineR: an R package for multivariate analysis. *J. Stat. Softw.* 25, 1–18.
- Leakey, M.G., 1993. Evolution of *Theropithecus* in the Turkana Basin. In: Jablonski, N.G. (Ed.), *Theropithecus: The Rise and Fall of a Primate Genus*. Cambridge University Press, Cambridge, pp. 85–123.
- Lebrun, R., Ponce de León, M., Tafforeau, P., Zollikofer, C., 2010. Deep evolutionary roots of strepsirrhine primate labyrinthine morphology. *J. Anat.* 216, 368–380.
- Macchiarelli, R., Bondioli, L., Mazurier, A., 2008. Virtual dentitions: touching the hidden evidence. In: Irish, J.D., Nelson, G.C. (Eds.), *Technique and Application in Dental Anthropology*. Cambridge University Press, Cambridge, pp. 426–448.
- Macchiarelli, R., Bayle, P., Bondioli, L., Mazurier, A., Zanolli, C., 2013. From outer to inner structural morphology in dental anthropology. The integration of the third dimension in the visualization and quantitative analysis of fossil remains. In: Scott, G.R., Irish, J.D. (Eds.), *Anthropological Perspectives on Tooth Morphology, Genetics, Evolution, Variation*. Cambridge University Press, Cambridge, pp. 250–277.
- Maier, W., 1970. New fossil Cercopithecoïdeia from the lower Pleistocene cave deposits of the Makapansgat Limeworks, South Africa. *Palaeont. Afr.* 13, 69–107.
- Maier, W., 1972. The first complete skull of *Simopithecus darti* from Makapansgat, South Africa, and its systematic position. *J. Hum. Evol.* 1, 395–405.
- Malinzak, M.D., Kay, R.F., Hullar, T.E., 2012. Locomotor head movements and semicircular canal morphology in primates. *Proc. Natl. Acad. Sci.* 109, 17914–17919.
- Manoussaki, D., Chadwick, R.S., Ketten, D.R., Arruda, J., Dimitriadis, E.K., O'Malley, J.T., 2008. The influence of cochlear shape on low-frequency hearing. *Proc. Natl. Acad. Sci.* 105, 6162–6166.
- Martin, L.B., 1985. Significance of enamel thickness in hominoid evolution. *Nature* 314, 260–263.
- McKee, J.K., 1993. Taxonomic and evolutionary affinities of *Papio izodi* fossils from Taung and Sterkfontein. *Palaeont. Afr.* 30, 43–49.
- McKee, J.K., Keyser, A.W., 1994. Craniodental remains of *Papio angusticeps* from the Haasgat Cave site, South Africa. *Int. J. Primatol.* 15, 823–841.
- McKee, J.K., von Mayer, A., Kuykendall, K., 2011. New species of *Cercopithecoïdes* from Haasgat, North West Province, South Africa. *J. Hum. Evol.* 60, 83–93.
- McGraw, W.S., Pampush, J.D., Daegling, D.J., 2012. Enamel thickness and durophagy in mangabeys revisited. *Am. J. Phys. Anthropol.* 147, 326–333.
- Mitteroecker, P., Bookstein, F.L., 2011. Linear discrimination, ordination, and the visualization of selection gradients in modern morphometrics. *Evol. Biol.* 38, 100–114.
- Mollett, O.D., 1947. Fossil mammals from the Makapan Valley, Potgietersrust. I. Primates. *S. Afr. J. Sci.* 43, 295–303.
- Olejniczak, A.J., Martin, L.B., Ulhaas, L., 2004. Quantification of dentine shape in anthropoid primates. *Ann. Anat.* 186, 479–485.
- Olejniczak, A.J., Gilbert, C.C., Martin, L.B., Smith, T.M., Ulhaas, L., Grine, F.E., 2007. Morphology of the enamel-dentine junction in sections of anthropoid primate maxillary molars. *J. Hum. Evol.* 53, 292–301.
- Olejniczak, A.J., Smith, T.M., Feeney, R.N.M., Macchiarelli, R., Mazurier, A., Bondioli, L., Rosas, A., Fordea, J., de la Rasilla, M., Garcia-Taberner, A., Radović, J., Skinner, M.M., Toussaint, M., Hublin, J.-J., 2008a. Dental tissue proportions and enamel thickness in Neandertal and modern human molars. *J. Hum. Evol.* 55, 12–23.
- Olejniczak, A.J., Smith, T.M., Skinner, M.M., Grine, F.E., Feeney, R.N.M., Thackeray, J.F., Hublin, J.-J., 2008b. Three-dimensional molar enamel distribution and thickness in *Australopithecus* and *Paranthropus*. *Biol. Lett.* 4, 406–410.
- Olejniczak, A.J., Tafforeau, P., Feeney, R.N.M., Martin, L.B., 2008c. Three-dimensional primate molar enamel thickness. *J. Hum. Evol.* 54, 187–195.
- R Development Core Team, 2015. R: a language and environment for statistical computing. <http://www.R-project.org>.
- Rook, L., Bondioli, L., Casali, F., Rossi, M., Köhler, M., Moyá Solá, S., Macchiarelli, R., 2004. The bony labyrinth of *Oreopithecus bambolii*. *J. Hum. Evol.* 46, 349–356.
- Shellis, R.P., Beynon, A.D., Reid, D.J., Hiiemae, K.M., 1998. Variations in molar enamel thickness among primates. *J. Hum. Evol.* 35, 507–522.
- Silcox, M.T., Bloch, J.I., Boyer, D.M., Godinot, M., Ryan, T.M., Spoor, F., Walker, A., 2009. Semicircular canal system in early primates. *J. Hum. Evol.* 56, 315–327.
- Skinner, M.M., Gunz, P., Wood, B.A., Hublin, J.-J., 2008. Enamel-dentine junction (EDJ) morphology distinguishes the lower molars of *Australopithecus africanus* and *Paranthropus robustus*. *J. Hum. Evol.* 55, 979–988.
- Spoor, C.F., 1993. The comparative morphology and phylogeny of the human bony labyrinth. Ph.D. Dissertation, University of Utrecht.
- Spoor, C.F., Hublin, J.-J., Braun, M., Zonneveld, F., 2003. The bony labyrinth of Neanderthals. *J. Hum. Evol.* 44, 141–165.
- Spoor, F., Zonneveld, F., 1998. Comparative review of the human bony labyrinth. *Yearb. Phys. Anthropol.* 41, 211–251.
- Spoor, F., Bajpai, S., Hussain, S.T., Kumar, K., Thewissen, J.G.M., 2002. Vestibular evidence for the evolution of aquatic behaviour in early cetaceans. *Nature* 417, 163–166.
- Spoor, F., Garland, T., Krovitz, G., Ryan, T.M., Silcox, M.T., Walker, A., 2007. The primate semicircular canal system and locomotion. *Proc. Natl. Acad. Sci.* 104, 10808–10812.
- Strait, D.S., Wood, B.A., 1999. Early hominid biogeography. *Proc. Natl. Acad. Sci.* 96, 9196–9200.
- Strasser, E., Delson, E., 1987. Cladistic analysis of cercopithecoïd relationships. *J. Hum. Evol.* 16, 81–99.
- Szalay, F.S., Delson, E., 1979. *Evolutionary History of the Primates*. Academic Press, New York.
- Thackeray, J.F., Myer, S., 2004. *Parapapio broomi* and *Parapapio jonesi* from Sterkfontein: males and females of one species? *Ann. Transv. Mus.* 41, 79–82.
- Tosi, A.J., Disotell, T.R., Morales, J.C., Melnick, D.J., 2003. Cercopithecoïd Y-chromosome data provide a test of competing morphological evolutionary hypotheses. *Mol. Phylogenet. Evol.* 27, 510–521.
- Toussaint, M., Olejniczak, A.J., El Zaatari, S., Cattelain, P., Flas, D., Letourneux, C., Piron, S., 2010. The Neandertal lower right deciduous second molar from Trou de l'Abîme at Couvin, Belgium. *J. Hum. Evol.* 58, 56–67.
- Williams, F.L., Ackermann, R.R., Leigh, S.R., 2007. Inferring Plio-Pleistocene southern biochronology from facial affinities in *Parapapio* and other fossil papionins. *Am. J. Phys. Anthropol.* 132, 163–174.
- Zanolli, C., Bondioli, L., Mancini, L., Mazurier, A., Widiyanto, H., Macchiarelli, R., 2012. Two human fossil deciduous molars from the Sangiran Dome (Java, Indonesia): outer and inner morphology. *Am. J. Phys. Anthropol.* 147, 472–481.
- Zanolli, C., Bondioli, L., Coppa, A., Dean, M.C., Bayle, P., Candilio, F., Capuani, S., Drossi, D., Fiore, I., Frayer, D.W., Libsekal, Y., Mancini, L., Rook, L., Medin Tekle, T., Tuniz, C., Macchiarelli, R., 2014. The late Early Pleistocene human dental remains from Uadi Aalad and Mulhuli-Amo (Buia), Eritrean Danakil: macromorphology and microstructure. *J. Hum. Evol.* 74, 96–113.